

1. Theory of Coherent Raman Scattering

Eric Olaf Potma and Shaul Mukamel

1.1	Introduction: The Coherent Raman Interaction	4
1.2	Nonlinear Optical Processes	5
1.2.1	Induced Polarization	5
1.2.2	Nonlinear Polarization	6
1.2.3	Magnitude of the Optical Nonlinearity	7
1.3	Classification of Raman Sensitive Techniques	8
1.3.1	Coherent versus Incoherent	8
1.3.2	Linear versus Nonlinear	8
1.3.3	Homodyne versus Heterodyne Detection	9
1.3.4	Spontaneous versus Stimulated	10
1.4	Classical Description of Matter and Field: The Spontaneous Raman Effect	10
1.4.1	Electronic and Nuclear Motions	10
1.4.2	Spontaneous Raman Scattering Signal	12
1.5	Classical Description of Matter and Field: Coherent Raman Scattering	13
1.5.1	Driven Raman Mode	14
1.5.2	Probe Modulation	15
1.5.3	Energy Flow in Coherent Raman Scattering	17
1.6	Semi-Classical Description: Quantum Matter and Classical Fields	21
1.6.1	Wavefunctions of Matter	21
1.6.2	Density Matrix	22
1.6.3	Response Functions and Third-Order Susceptibility	25
1.6.3.1	Material Response Function	25
1.6.3.2	Third-Order Susceptibility	26
1.6.3.3	Frequency Dependence of $\chi^{(3)}$	29
1.6.3.4	Spatial Polarization Properties of $\chi^{(3)}$	30
1.7	Quantum Description of Field and Matter	31
1.7.1	Quantum Description of the Field	32
1.7.1.1	Field Perspective	33
1.7.1.2	Material Perspective	34
1.7.2	Quantum Description of Spontaneous Raman Scattering	35

1.7.3 Quantum Description of Coherent Raman Signals: Interference of Pump-Probe Paths	37
1.7.4 Quantum Description of Heterodyne Coherent Raman Signals	38
1.8 Concluding Remarks	41
Acknowledgments	41
References	41

1.1 Introduction: The Coherent Raman Interaction

The term “coherent Raman scattering” (CRS) denotes a special class of light-matter interactions. Central to this class of interactions is the particular way in which the material is responding to the incoming light fields: the response contains information about material oscillations at difference frequencies of two incident light fields. Hence, writing the frequencies of the light fields as ω_1 and ω_2 , the coherent Raman interaction depends on oscillatory motions in the material at the frequency $\Omega = \omega_1 - \omega_2$. This simple stipulation dresses coherent Raman techniques with many unique capabilities. In particular, since the difference frequency Ω generally corresponds to a low frequency oscillation which can be tuned into resonance with characteristic vibrational modes ω_v , coherent Raman techniques make it possible to probe the low frequency nuclear vibrations of materials and molecules by using high frequency optical light fields.

Coherent Raman techniques are related to spontaneous Raman scattering. In spontaneous Raman scattering, a single ω_1 mode is used to generate the ω_2 mode, which is emitted spontaneously. Both coherent and spontaneous Raman scattering allow for vibrational spectroscopic examination of molecules with visible and near-infrared radiation.

Compared to spontaneous Raman scattering, CRS techniques can produce much stronger vibrationally sensitive signals. The popularity of CRS techniques in optical microscopy is intimately related to these much improved signal levels, which have enabled the fast scanning capabilities of CRS microscopes. However, beyond stronger vibrational signals, the coherent Raman interaction offers a rich palette of probing mechanisms for examining a wide variety of molecular properties. In general, CRS techniques offer a more detailed control of the Raman response of the medium than what is available through spontaneous Raman techniques. CRS allows a more direct probing of the molecular coherences that govern the Raman vibrational response. When ultrafast pulses are used, CRS methods can resolve the ultrafast evolution of such Raman coherences on the appropriate timescale. CRS techniques also offer more detailed information about molecular orientation than spontaneous Raman techniques. In addition, advanced resonant Raman (coherent or spontaneous) techniques can selectively probe both the electronic and vibrational response of the material, which opens a window to a wealth of molecular information.

In this chapter, we examine the basics of the coherent Raman interaction, which provides a foundation for more advanced topics discussed in subsequent chapters of this book. Here, we focus predominantly on the light-matter interaction itself. We study both the classical and the semi-classical descriptions of the coherent Raman process and discuss strengths and weaknesses of each approach. In addition, we highlight some of

the findings obtained with a quantum mechanical model of the CRS process. The propagation of light in the material, which gives rise to several interesting effects in coherent Raman microscopy in the tight focusing limit, is discussed in Chapter 2.

1.2 Nonlinear Optical Processes

1.2.1 Induced Polarization

Both linear and nonlinear optical effects can be understood as resulting from the interaction of the electric field component of electromagnetic radiation with the charged particles of the material or molecule. Generally, an applied electric field moves positively charged particles in the direction of the field and negative charges in the opposite direction. The electric field associated with the visible and near-infrared range of the electromagnetic spectrum oscillates at frequencies in the 10^3 THz range. Such driving frequencies are too high for the nuclei to follow adiabatically. The electrons in the material or molecule, however, are light enough to follow the rapid oscillations of the driving field. Consequently, optical resonances in this frequency range are predominantly due to the motions of the electrons in the material.

As a result of the driving fields, the bound electrons are slightly displaced from their equilibrium positions, which induces an electric dipole moment:

$$\mu(t) = -e \cdot r(t) \quad (1.1)$$

where e is the charge of the electron. The magnitude of the dipole depends on the extent of the displacement $r(t)$. The displacement, in turn, is dependent on how strong the electron is bound to the nuclei. The displacement will be more significant for electrons that are weakly bound to the nuclei, and smaller for electrons that are tightly bound. Close to the nuclei, the electron binding potential can generally be approximated by a harmonic potential.

The macroscopic polarization, which is obtained by adding up all N electric dipoles per unit volume, reads:

$$P(t) = N\mu(t) \quad (1.2)$$

In the limit of weak applied electric fields (compared to the field that binds the electrons to the nuclei), the displacement is directly proportional to the electric field. This allows us to write the polarization as:

$$P(t) = \epsilon_0 \chi E(t) \quad (1.3)$$

where

ϵ_0 is the electric permittivity in vacuum

χ is the susceptibility of the material (we will use SI units unless otherwise stated)

This expression highlights that, in the weak field limit, the induced polarization in the material depends linearly on the magnitude of the applied field. Such linear dependence is the origin of all linear optical phenomena.

1.2.2 Nonlinear Polarization

For stronger fields, the electron is farther displaced from its equilibrium position. For larger displacements, the binding potential can no longer be assumed to be harmonic as anharmonic effects become more significant. When the anharmonic shape of the potential becomes important, the dependence between the driving electric field and the induced polarization is not strictly linear, and corrections to the polarization will have to be made. **Figure 1.1** illustrates the nonlinearity between the driving field and the induced polarization in the presence of anharmonicity. If the anharmonic contributions to the harmonic potential are relatively small, the displacement r can be expressed as a power series in the field. This implies that the displacement of the electron is no longer linearly dependent on the field as nonlinear corrections grow in importance. In a similar fashion, the polarization can be written as a power series in the field to include the nonlinear electron motions:

$$\begin{aligned} P(t) &= \epsilon_0[\chi^{(1)}E(t) + \chi^{(2)}E^2(t) + \chi^{(3)}E^3(t) + \dots] \\ &= P^{(1)}(t) + P^{(2)}(t) + P^{(3)}(t) + \dots \end{aligned} \quad (1.4)$$

where

$\chi^{(n)}$ is the n th order susceptibility

$P^{(n)}$ is the n th order contribution to the polarization

The coherent Raman effects described in this book can all be understood as resulting from the third-order contribution to the polarization $P^{(3)}$. The magnitude of these effects is thus governed by the strength of the triple product of the incoming fields and the amplitude of the third-order susceptibility $\chi^{(3)}$.

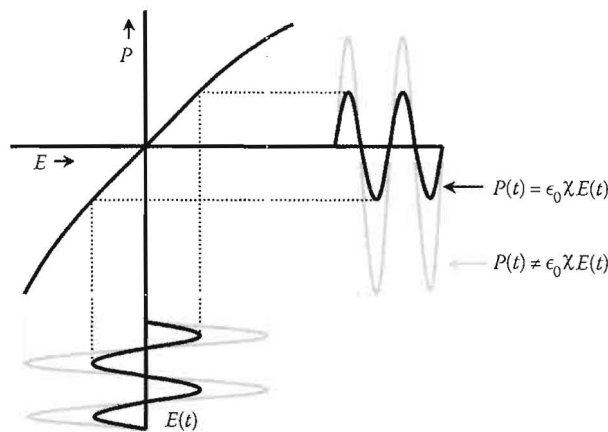


FIGURE 1.1 Relation between incident electric field and the induced polarization. For weak electric fields, indicated by the black sinusoidal line, only the harmonic part of the potential is relevant and the polarization depends linearly on the field. For strong electric fields, symbolized by the gray sinusoidal line, the anharmonicities of the potential contribute and the polarization depends nonlinearly on the incoming field. In this case, the polarization profile no longer matches the profile of the sinusoidal input modulation.

1.2.3 Magnitude of the Optical Nonlinearity

To appreciate the nonlinear origin of coherent Raman effects, it is useful to examine the magnitude of the third-order susceptibility. From the previous discussion it follows that the nonlinearity results predominantly from the electronic anharmonic electron motions. This is indeed the case when ultrafast pulses in the picosecond to the femtosecond range are used, which induce nonlinear optical effects that are typically directly related to the electronic polarizability of the material. We may expect that the nonlinear electron motions become very significant when the applied field is of the order of the field that binds the electron to the atom. This atomic field is $E_a \approx 2 \times 10^7$ esu (in electrostatic units). Hence, in case the applied field is of the order of E_a we expect the nonlinear polarization to be comparable to the linear polarization, i.e., $P^{(1)} \approx P^{(3)}$. Under these (nonresonant) conditions we can write $\chi^{(1)}E_a \approx \chi^{(3)}E_a^3$ and thus estimate that $\chi^{(3)} \approx \chi^{(1)}/E_a^2$. Given that $\chi^{(1)}$ is about unity in the condensed phase, this yields a numerical value for the nonresonant third-order susceptibility of $\chi^{(3)} \simeq 3 \times 10^{-15}$ [1]. Despite the approximate nature of this estimate, it is surprisingly close to actual measurements of the nonlinear susceptibility. Numerical values of some materials and compounds are given in Table 1.1.

Table 1.1 Magnitude of $\chi^{(3)}$ as Determined with Third-Harmonic Generation Measurements at the Indicated Excitation Wavelength

Material	$\chi^{(3)}$ (esu)	λ (μm)	Reference
Water	1.3×10^{-14}	1.06	[2]
Glycine (1 M aqueous)	1.2×10^{-14}	1.06	[2]
Ethanol	1.3×10^{-14}	1.06	[2]
Vegetable oil	1.9×10^{-14}	1.06	[2]
Carbon disulfide	2.0×10^{-13}	1.91	[3]
Silica	1.4×10^{-14}	1.06	[4]
BK7	2.1×10^{-14}	1.06	[4]
TiO ₂ (rutile)	4.0×10^{-12}	1.90	[5]

To generate an observable third-order optical signal in practice, applied fields are used that are generally much weaker than E_a . This condition is required because otherwise the $\chi^{(3)}$ response cannot be easily isolated from higher order nonlinearities. In addition, fields of the order of E_a would correspond to laser intensities of $\sim 10^{14}$ W cm⁻², which is many orders of magnitude too high for applications in microscopy. At the much lower laser intensities relevant to laser scanning optical microscopy ($\sim 10^{10}$ W cm⁻²), the third-order response is orders of magnitude smaller than the linear response, but can nonetheless be detected.

The magnitude of $\chi^{(3)}$ grows larger whenever the electron displacement is enhanced. This is the case under electronically resonant conditions. When the frequency of the driving field is tuned to the frequency of an electronic resonance in the material or molecule, we may expect that the electron displacement is magnified and the third-order

nonlinear response is correspondingly stronger. This principle is utilized, for instance, in four-wave mixing microscopy of nanostructures where strong $\chi^{(3)}$ -based signals are attained through electronic resonances [6]. In addition to electronic resonances, the presence of nuclear resonances can also affect the electronic nonlinear susceptibility. The coherent Raman effects discussed in this book all derive their chemical sensitivity from these nuclear resonances. In the following sections, we will first introduce a general classification of Raman sensitive techniques, followed by a discussion on the classical Raman effect and the manifestation of the Raman effect in the coherent nonlinear response of the material.

1.3 Classification of Raman Sensitive Techniques

Before we discuss the basics of the Raman effect, it is useful to define a couple of terms that will prove useful for interpreting the different types of optical techniques for probing the Raman effect.

1.3.1 Coherent versus Incoherent

An important classification is whether the detected signal is coherent or incoherent. The signal is coherent if the optical waves radiated from dipole emitters at different points \mathbf{r} in the sample exhibit a well-defined phase relationship. In this case, the total field, obtained by averaging over all dipole emitters, is non-vanishing and thus $\langle E \rangle \neq 0$. On the other hand, if the phases of the emitted waves are random relative to one another, then the total field averages to zero, i.e., $\langle E \rangle = 0$. This latter case represents an incoherent signal. Note that even though the total field is zero for incoherent signals, the intensity defined by $\langle E^*E \rangle$ can be finite.

Conventional spontaneous Raman scattering is an example of an incoherent signal, because the phase of the wave radiated by an individual molecule is uncorrelated with the waves emitted by other molecules in the sample. Rayleigh (elastic) scattering, on the other, is a coherent signal. In Rayleigh scattering, the phase of the scattered waves is not perturbed by a nuclear mode with arbitrary phase, producing scattered radiation with a definite phase relation relative to the incoming waves. The difference between Raman scattered light and Rayleigh scattered light is further addressed in Section 1.4.2. All nonlinear Raman techniques produce coherent signals. Contrary to incoherent Raman, in nonlinear Raman techniques the nuclear oscillators in the sample are correlated by the light fields, producing radiation from different points in the sample with a well-defined phase relationship. All nonlinear Raman techniques discussed in the book are classified as coherent.

1.3.2 Linear versus Nonlinear

The linearity of the signal is defined through its dependence on the intensity I of the incident radiation. Optical signals that scale linearly with the average power of the incident radiation are classified as linear techniques. Optical signals that exhibit a quadratic or higher order dependence on the intensity of the input radiation are classified as nonlinear techniques. Incoherent (spontaneous) Raman is linear, whereas CRS techniques

Table 1.2 Classification of Raman Sensitive Techniques

	Incoherent	Coh. Homodyne CARS	Coh. Heterodyne CARS	Pump-Probe
Common name	Spontaneous Raman	CARS	Heterodyne CARS	SRS
Raman resonance	Spontaneous	Stimulated	Stimulated	Stimulated
Detection mode	Spontaneous	Spontaneous	Stimulated	Stimulated
N scaling	N	N^2	N	N
I scaling	I	I^3	I^2	I^2

N denotes number density of Raman scatterers and I denotes intensity of the incident radiation.

are nonlinear. The intensity dependence of different Raman sensitive techniques is listed in Table 1.2. The linearity of the optical signal with respect to its dependence on I should not be confused with the linearity of the light-matter interaction. For example, although incoherent Raman is a linear technique, it can be described as a nonlinear interaction between photon fields and the material.

1.3.3 Homodyne versus Heterodyne Detection

A further classification of the signal is based on the way it is detected. In terms of classical fields, if the sample radiation is detected at an optical frequency different from the incident radiation, the signal intensity is proportional to $|E|^2$. In this case, the signal is classified as homodyne, as the intensity is the square modulus of the emitted field itself. If the emitted field occurs at a frequency that is identical to any of the frequencies contained in the incident radiation E_{in} , then the signal intensity is proportional to $|E + E_{in}|^2$. Consequently, the detected intensity contains a mixing term, i.e., $E^* E_{in} + E E_{in}^*$. We define this mixing term as the heterodyne contribution to the signal, as the emitted field is mixed with another field. In terms of quantized fields, the signal is homodyne if detected at a field mode that is initially vacant and heterodyne when detected at a field mode that is already occupied. Note that the current definition, which is commonly used to describe the detection method in molecular spectroscopy, is different from the definition used in the quantum optics and optical engineering literature. In this book, we will use the spectroscopy definition of homodyne and heterodyne signals because it is better suited to classify the different Raman sensitive techniques in a comprehensive fashion.

For instance, conventional coherent anti-Stokes Raman scattering (CARS) is a coherent homodyne technique. It is coherent because the waves emitted from different points in the sample exhibit a definite phase relation, and the detection is homodyne because the detected signal at the anti-Stokes frequency occurs at a field mode different from the input fields. In heterodyne CARS, the emitted field is mixed with another field at the anti-Stokes frequency, usually called local oscillator, and the mutual interference of the fields is detected. The interferometric mixing term is the heterodyne contribution to the signal. In case the one of the incident excitation fields acts as the local oscillator, i.e., detection occurs at a frequency similar to one of the input fields, the signal is self-heterodyned. Raman sensitive pump-probe is an example of a self-heterodyned signal, which is a

special case of the heterodyne coherent Raman technique. Raman sensitive pump-probe is commonly called stimulated Raman scattering (SRS), in which the signal is detected at a field mode already occupied by one of the input fields. The designator *stimulated* is, however, somewhat misleading since it is not unique to SRS, as other coherent Raman techniques also have a stimulated component. We address this issue below.

1.3.4 Spontaneous versus Stimulated

We can define the stimulated character of Raman sensitive techniques at two levels. The first level pertains to the way the Raman resonance is created. Classically, if the Raman active molecule is driven into resonance by two incident (off-resonance) fields, the Raman resonance is said to be stimulated. The initial phase of the Raman oscillation is determined by the relative phase difference of the input fields. In all nonlinear Raman techniques the Raman resonance is driven in a stimulated fashion. If the molecule is addressed with one (off-resonance) input field, the Raman resonance is established in a spontaneous manner. The phase of the Raman oscillation is determined by the random phases of the nuclear oscillators at equilibrium. This case describes the Raman resonance relevant to incoherent Raman techniques.

The second level relates to the mechanism of detection. This level is best explained in terms of quantized fields. If the field is detected at a field mode that is initially vacant, then the detected signal is spontaneous. This case represents both incoherent Raman techniques and homodyne detected coherent Raman techniques. In both cases, the detection mode is at an optical frequency different from the frequencies carried by the input fields. Note that if a signal is spontaneous in the detection mode, it is not necessarily incoherent. For instance, homodyne CARS is spontaneous in the detection mode, but the detected signal is coherent. If the field is detected at a field mode that is occupied by one of the input fields, then the signal is classified as stimulated. Heterodyne coherent Raman techniques, including Raman sensitive pump-probe, are stimulated in the detection mode. Hence, both heterodyne CARS and SRS are stimulated in the detection mode. In this regard, the term SRS does not exclusively cover the traditional stimulated Raman loss (SRL) or stimulated Raman gain techniques (SRG), as it encompasses more coherent Raman techniques as well. Therefore, a better classification for SRL and SRG techniques would be Raman sensitive *pump-probe*, which more accurately captures the nature of the detected signal. In the remainder of this chapter, we will refer the techniques by their common names (see Table 1.2), but the reader is warned about the existing ambiguities in the current nomenclature.

1.4 Classical Description of Matter and Field: The Spontaneous Raman Effect

1.4.1 Electronic and Nuclear Motions

Although it is the electrons in the molecule that are set in motion by the visible or near-IR driving fields, their oscillatory motions do contain information about the motions of nuclei. The reason for this is that the adiabatic electronic potential depends on the nuclear coordinates. Since the electrons are bound to the nuclei,

nuclear motions will affect the motions of the electrons as well. Hence, the electronic polarizability is perturbed by the presence of nuclear modes. To describe the effect of the nuclear motions, we first connect the electric dipole moment to the polarizability $\alpha(t)$ under the assumption that the driving frequency is far from any electronic resonances of the system:

$$\mu(t) = \alpha(t)E(t) \quad (1.5)$$

In the hypothetical absence of nuclear modes and/or nonlinearities, the polarizability can be approximated as a constant α_0 . In the presence of nuclear modes, we can express the electronic polarizability in terms of the nuclear coordinate Q , and expand it in a Taylor series [7]:

$$\alpha(t) = \alpha_0 + \left(\frac{\delta\alpha}{\delta Q} \right)_0 Q(t) + \dots \quad (1.6)$$

The first-order correction to the polarizability has a magnitude of $\delta\alpha/\delta Q$ and can be interpreted as the coupling strength between the nuclear and electronic coordinates. The nuclear motion along Q can be assumed to be that of a classical harmonic oscillator:

$$Q(t) = 2Q_0 \cos(\omega_v t + \phi) = Q_0 \left[e^{i\omega_v t + i\phi} + e^{-i\omega_v t - i\phi} \right] \quad (1.7)$$

where

Q_0 is the amplitude of the nuclear motion

ω_v is the nuclear resonance frequency

ϕ is the phase of the nuclear mode vibration

When the incoming field is written as $E(t) = Ae^{-i\omega_1 t} + \text{c.c.}$, then the dipole moment is found as:

$$\mu(t) = \alpha_0 A e^{-i\omega_1 t} + A \left(\frac{\delta\alpha}{\delta Q} \right)_0 Q_0 \left\{ e^{-i(\omega_1 - \omega_v)t + i\phi} + e^{-i(\omega_1 + \omega_v)t - i\phi} \right\} + \text{c.c.} \quad (1.8)$$

The dipole moment oscillates at several frequencies. The first term on the right-hand side of Equation 1.8 describes the process of elastic Rayleigh scattering at the incident frequency. The second term describes the inelastic Raman-shifted frequencies at $\omega_1 - \omega_v$, which is called the Stokes-shifted contribution, and at $\omega_1 + \omega_v$, the anti-Stokes-shifted contribution. The scattering process is illustrated in **Figure 1.2**. Note that the Raman term is directly proportional to $\delta\alpha/\delta Q$, which describes how the applied field brings about a polarizability change along the nuclear mode. The polarizability change is strongly dependent on the symmetry of the nuclear mode in the molecule, which forms the basis for the selection rules in Raman spectroscopy.

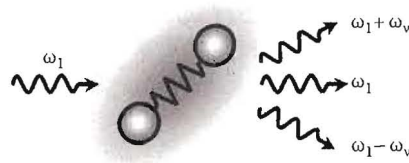


FIGURE 1.2 Schematic of spontaneous Raman scattering. The incoming light is scattered at the molecule into a Rayleigh component at ω and two Raman-shifted components at $\omega - \omega_v$ and $\omega + \omega_v$, the Stokes and anti-Stokes contributions, respectively.

1.4.2 Spontaneous Raman Scattering Signal

Within the classical model for Raman scattering, the harmonic nuclear mode dresses the oscillating dipole with frequency-shifted components. The amplitude of the Stokes and anti-Stokes components are then proportional to the magnitude of the electric field radiated by the dipole at the shifted frequencies. It is instructive to examine the magnitude of the Raman-shifted signal within the framework of the classical model. We will consider the Stokes-shifted component at $\omega_s = \omega_1 - \omega_v$. The derivation of the anti-Stokes component is similar.

The amplitude of the electric field at frequency ω_s , radiated by the oscillating dipole along \mathbf{r} in the far field, is obtained from electrodynamics in scalar form as:

$$E(\omega_s) = \frac{\omega_s^2}{4\pi\epsilon_0 c^2} |\mu(\omega_s)| \frac{e^{ikr}}{r} \sin\theta \tag{1.9}$$

where

- k is the wave vector of the radiated field
- c is the speed of light
- θ is the angle relative to the dipole axis
- r is the distance from the dipole location to the observation point
- $|\mu(\omega_s)|$ is the amplitude of the dipole oscillation at ω_s

The outgoing energy flux along \mathbf{r} is calculated as the time-averaged Poynting flux S :

$$S(\omega_s) = \frac{\epsilon_0 c}{2} |E(\omega_s)|^2 \tag{1.10}$$

The total energy radiated by the (single) dipole is then obtained by integrating the energy flux over the unit sphere. Using $|\mu(\omega_s)|$ from Equation 1.8, the intensity of the Raman-shifted light is:

$$I(\omega_s) = \frac{\omega_s^4}{12\pi\epsilon_0 c^3} Q_0^2 |A|^2 \left| \frac{\delta\alpha}{\delta Q} \right|^2 \tag{1.11}$$

From Equation 1.11 we see that the classical model predicts a ω^4 dependence of the intensity of the Raman scattered light. In addition, it scales with $|\delta\alpha/\delta Q|^2$ and with the intensity of the incident beam $I_0 = |A|^2$. The phase ϕ of the Raman scattered light is dependent on the nuclear mode oscillation. At equilibrium, the nuclear vibrations of different molecules are uncorrelated, i.e., each molecule i carries its own independent phase ϕ_i . This implies that the phase of the radiated field from one dipole emitter is unrelated to the phase of the radiated field by a second dipole emitter elsewhere in the sample. Consequently, the signal is incoherent and the intensity of the total Raman emission is proportional to Equation 1.11 multiplied by the total number of Raman scatterers in the sample. It is interesting to note that the first term in Equation 1.8, which represents elastic light scattering, is not dependent on the nuclear vibration, and thus does not acquire a random phase ϕ . This is the reason why Rayleigh scattering is coherent while the Raman-shifted contributions are incoherent.

Experimentally it is useful to define the Raman signal strength in terms of a cross section. The cross section expresses the Raman scattering efficiency of a molecule in a manner analogous to describing light absorption through the absorption cross section (Beer's law). Using the cross section σ , the total scattered Raman-shifted light from a sample with length z and a molecular number density N is written as:

$$I(\omega_s) = Nz\sigma(\omega_s)I_0 \quad (1.12)$$

Comparing Equations 1.12 and 1.11, it is evident that the Raman cross section is directly proportional to $|\delta\alpha/\delta Q|^2$. This underlines the central importance of the condition of a non-zero polarizability change along the nuclear coordinate.

Unfortunately, the classical model does not offer a correct description of the resonance behavior of the polarizability. In addition, the classical description is unable to predict the ratio between the intensities of the Stokes and anti-Stokes contributions. A quantum mechanical treatment of the molecule is required to account for these effects. Furthermore, because the field is treated classically, the amount of energy exchange between the light fields and the molecule cannot be accurately described, and some corrections to Equation 1.11 are needed. We will address these issues in Section 1.7.2.

Despite these shortcomings, the classical model provides a useful physical picture for interpreting several attributes of the spontaneous Raman scattering process and the coherent Raman scattering process alike. In the next section, we will highlight some of the basic properties of coherent Raman techniques in the context of the classical description.

1.5 Classical Description of Matter and Field: Coherent Raman Scattering

The classical description of the coherent Raman effect provides an intuitive interpretation of the light-matter interaction in terms of actively driven nuclear oscillations in the material. For clarity, the following derivation assumes a single harmonic nuclear mode per molecule. Even though this description does no justice to the multitude of vibrational states of actual molecules, it introduces a clear picture in which a driven nuclear mode forms the source for coherent scattering of light. Extending the description to include multiple modes is straightforward.

Briefly, this description divides the coherent Raman process into two steps. First, two incoming fields induce oscillations in the molecular electron cloud. These oscillations form an effective force along the vibrational degree of freedom, which actively drives the nuclear modes. Second, the driven nuclear mode forms the source of a spatially coherent modulation of the material's refractive properties. A third light field, which propagates through the material and experiences this modulation, will develop sidebands that are shifted by the modulation frequency. The amplitude of the field scattered into these sidebands forms the basis of the frequency-shifted coherent Raman signal. Below we will discuss the key elements of the classical model.

1.5.1 Driven Raman Mode

In the classical model for the coherent Raman process, we assume that the vibrational motion in the molecule can be described by a damped harmonic oscillator with a resonance frequency ω_v . Similar to the situation encountered in the classical description of the spontaneous Raman process, we can think of the oscillator as the vibrational motion of two nuclei along their internuclear axis Q . This system is subject to two incoming light fields E_1 and E_2 , which are modeled as plane waves:

$$E_i(t) = A_i e^{-i\omega_i t} + \text{c.c.} \quad (1.13)$$

where the subscript $i = (1, 2)$ and all propagation factors are included in the amplitude A_i . As before, we assume that the frequencies ω_1 and ω_2 are much higher than the resonance frequency ω_v , and that $\omega_1 > \omega_2$. Since the incident frequencies are far from the resonance frequency of the oscillator, the nuclear mode will not be driven efficiently by the fundamental fields. The electrons surrounding the nuclei, however, can follow the incident fields adiabatically. In addition, when the fields are sufficiently intense, nonlinear electron motions can occur at combination frequencies, including the difference frequency $\Omega = \omega_1 - \omega_2$. Under these conditions, the combined optical field exerts a force on the vibrational oscillator:

$$F(t) = \left(\frac{\delta\alpha}{\delta Q} \right)_0 \left[A_1 A_2^* e^{-i(\Omega)t} + \text{c.c.} \right] \quad (1.14)$$

From Equation 1.14 we see that, because the electronic motions are coupled to the nuclear motions through a nonzero $(\delta\alpha/\delta Q)_0$, the modulated electron cloud introduces a time-varying force that oscillates at the difference frequency Ω and which is felt by the nuclear mode. In the presence of the driving fields, the nuclear displacement Q can then be expressed by the following equation of motion [8]:

$$\frac{d^2 Q(t)}{dt^2} + 2\gamma \frac{dQ(t)}{dt} + \omega_v Q(t) = \frac{F(t)}{m} \quad (1.15)$$

where

γ is the damping constant

m indicates the reduced mass of the nuclear oscillator

ω_v is the resonance frequency of the harmonic nuclear mode

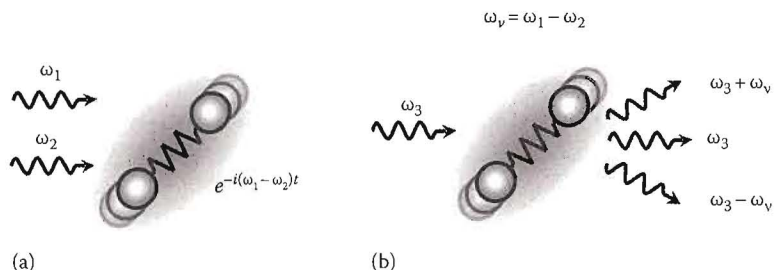


FIGURE 1.3 Schematic of coherent Raman scattering. (a) Two incoming fields drive a harmonic oscillator at the difference frequency $\Omega = \omega_1 - \omega_2$. (b) The presence of this oscillation causes a fluctuating refractive index for a third field ω_3 , which develops sidebands that are shifted Ω from the fundamental frequency. The amplitude of the sidebands is maximized when Ω equals the resonance frequency ω_v of the oscillator, which yields sidebands at $\omega_3 + \omega_v$ and $\omega_3 - \omega_v$.

The time-varying nuclear displacement can be found from Equation 1.15 as:

$$Q(t) = Q(\Omega)e^{-i\Omega t} + c.c. \quad (1.16)$$

which oscillates at Ω with the amplitude:

$$Q(\omega_v) = \frac{1}{m} \left(\frac{\delta\alpha}{\delta Q} \right)_0 \frac{A_1 A_2^*}{\omega_v^2 - \Omega^2 - 2i\Omega\gamma} \quad (1.17)$$

The physical interpretation of Equation 1.17 is clear. The nuclear mode is driven by the joint action of the incident fields. The amplitude of the vibrational motion depends on the amplitudes of the applied light fields and the magnitude of the coupling of the nuclear coordinate to the electronic polarizability $(\delta\alpha/\delta Q)_0$. The extent of the vibration also depends on the difference between the effective driving frequency Ω and the resonance frequency ω_v of the oscillator. Indeed, the amplitude of the oscillatory motion is largest when the difference frequency Ω matches the oscillator's resonance frequency (Figure 1.3).

1.5.2 Probe Modulation

The presence of the driven nuclear motion affects the optical properties of the material. As a consequence, the applied electric fields E_1 and E_2 will experience a slightly altered electronic polarizability upon propagating through the material. The effective macroscopic polarization in the material is the sum of the dipole moments as in Equation 1.2.

Using Equations 1.2, 1.5, and 1.6 we can write the polarization as:

$$P(t) = N \left[\alpha_0 + \left(\frac{\delta\alpha}{\delta Q} \right)_0 Q(t) \right] \{E_1(t) + E_2(t)\} \quad (1.18)$$

The terms proportional to α_0 correspond to the linear polarization of the material, whereas the terms proportional to $(\delta\alpha/\delta Q)_0$ describe the contribution to the third-order polarization due to the driven Raman mode. This latter contribution is the nonlinear polarization, which, using Equations 1.13 and 1.16, can be written as:

$$P_{NL}(t) = P(\omega_{cs})e^{-i\omega_{cs}t} + P(\omega_2)e^{-i\omega_2t} + P(\omega_1)e^{-i\omega_1t} + P(\omega_{as})e^{-i\omega_{as}t} + \text{c.c.} \quad (1.19)$$

where

$\omega_{cs} \equiv 2\omega_2 - \omega_1$ is referred to as the coherent Stokes frequency

$\omega_{as} \equiv 2\omega_1 - \omega_2$ is referred to as the anti-Stokes frequency

The nonlinear polarization thus contains contributions that oscillate at the fundamental frequencies ω_1 and ω_2 , as well as contributions that oscillate at the new frequencies ω_{cs} and ω_{as} . The relation between these frequency components is sketched in **Figure 1.4**. The amplitude of the polarization at the anti-Stokes frequency is given by:

$$P(\omega_{as}) = \frac{N}{m} \left(\frac{\delta\alpha}{\delta Q} \right)_0^2 \frac{1}{\omega_v^2 - \Omega^2 - 2i\Omega\gamma} A_1^2 A_2^* = 6\epsilon_0 \chi_{NL}(\Omega) A_1^2 A_2^* \quad (1.20)$$

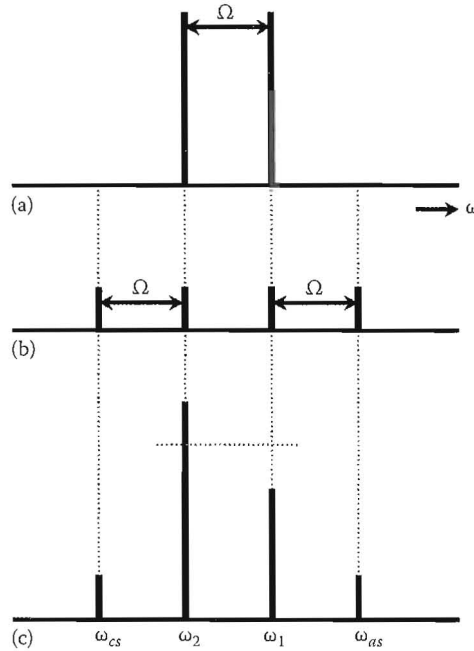


FIGURE 1.4 Spectrum of the coherent Raman components. (a) Incident (narrow band) frequencies at ω_1 and ω_2 . (b) Each input frequency develops side bands shifted by $\pm\Omega$, producing ω_{cs} and ω_1 for the ω_2 input frequency, and ω_2 and ω_{as} for the ω_1 input frequency. (c) The intensities of the coherent Raman components after passage through the sample. The ω_2 frequency channel has experienced a gain and the ω_1 frequency channel has experienced a loss.

where the nonlinear susceptibility is defined as:

$$\chi_{NL}(\Omega) = \frac{N}{6m\epsilon_0} \left(\frac{\delta\alpha}{\delta Q} \right)_0 \frac{1}{\omega_v^2 - \Omega^2 - 2i\Omega\gamma} \quad (1.21)$$

Similarly, we can write for the other frequency components:

$$P(\omega_{cs}) = 6\epsilon_0 \chi_{NL}^*(\Omega) A_2^2 A_1^* \quad (1.22)$$

$$P(\omega_2) = 6\epsilon_0 \chi_{NL}^*(\Omega) |A_1|^2 A_2 \quad (1.23)$$

$$P(\omega_1) = 6\epsilon_0 \chi_{NL}(\Omega) |A_2|^2 A_1 \quad (1.24)$$

The nonlinear polarizations given in Equations 1.20 through 1.24 describe the four lowest order coherent Raman effects: $P(\omega_{cs})$ is responsible for coherent Stokes Raman scattering (CSRS), $P(\omega_2)$ for stimulated Raman gain (SRG), $P(\omega_1)$ for stimulated Raman loss (SRL), and $P(\omega_{as})$ for coherent anti-Stokes Raman scattering (CARS). We see that the amplitudes of the different nonlinear polarization components all depend on the magnitude of the same χ_{NL} . Therefore, the material polarizations of the four coherent Raman effects are comparable in magnitude: they are all induced by the same nuclear vibration at ω_v . However, this does not imply that the actual detected signals of the four CRS techniques are of similar strength. We will discuss this issue in next section.

1.5.3 Energy Flow in Coherent Raman Scattering

As we have seen in the previous section, the induced polarization in the material produces radiation at the fundamental frequencies and at two new frequencies ω_{cs} and ω_{as} . In the coherent Raman process, energy contained in the fundamental light fields is redirected in two ways. First, there is an energy exchange with the material. In the presence of the driving fields, the material can either gain or lose energy. In case the total energy contained in all the light fields combined is lower after passing through the material, the total energy of the material will be higher. This type of process is called *dissipative*. Second, new light fields can be generated without energy exchange with the material. In this latter process, energy amounts formed by adding and subtracting the incoming light fields are used to generate new light fields while the material acts merely as a mediator. In these so-called *parametric* processes, the total energy of the combined light fields is conserved.

To describe energy flow in the classical model, explicit evaluation of Maxwell's wave equation is required, which connects the induced polarization to a radiating coherent field. All participating waves (ω_1 , ω_2 , ω_{cs} , ω_{as}) need to be taken into account in a coupled wave equation approach [9]. The coupled equations are then integrated over the (macroscopic) volume that contains the molecules in order to find the energy exchange between the waves and the material as well as the energy exchange among the waves. Such a derivation is beyond the scope of this chapter. Here we wish to highlight the

essentials of energy flow in coherent Raman processes without explicitly incorporating wave propagation effects. The following discussion is, therefore, qualitative in nature. Wave propagation is discussed in detail in Chapter 2.

We first discuss the case of homodyne detection. We will start our discussion with considering the fields at the new frequencies ω_{as} and ω_{cs} . The nonlinear field at the anti-Stokes frequency can be written as:

$$E_{as}^{(3)}(t) = A_{as} e^{-i\omega_{as}t} + c.c. \quad (1.25)$$

The corresponding intensity associated with this field is given by:

$$I(\omega_{as}) = \frac{\epsilon_0 c}{2} |A_{as}|^2 \quad (1.26)$$

In the lowest order coherent Raman interaction, the only source for the anti-Stokes field is the nonlinear polarization that oscillates at ω_{as} . The magnitude of the anti-Stokes field A_{as} is thus proportional to the magnitude of $P(\omega_{as})$. Using Equation 1.20, we can then write:

$$I(\omega_{as}) \propto |\chi_{NL}|^2 I_1^2 I_2 \quad (1.27)$$

where I_1 and I_2 are the intensities of the beams at ω_1 and ω_2 , respectively. Similarly, we find for the intensity of the coherent Stokes contribution:

$$I(\omega_{cs}) \propto |\chi_{NL}|^2 I_2^2 I_1 \quad (1.28)$$

In the above description, the coherent Stokes and anti-Stokes contributions are detected as homodyne signals, i.e., the signals are directly proportional to the modulus square of the nonlinear polarization. In this limit, the energy contained in the ω_{cs} and ω_{as} frequency channels is extracted from the incident fields at ω_1 and ω_2 , as can be shown by performing a coupled wave equation analysis [9]. Because the process is parametric, no effective energy exchange with the material has taken place.

The situation changes when an additional field at frequency ω_{cs} or ω_{as} is applied to the material. This additional field is commonly referred to as a *local oscillator*, which must exhibit a well-behaved phase relation with the nonlinear polarization in the material. In the presence of a local oscillator, the induced nonlinear polarization is no longer the only source of radiation at the signal frequency. The intensity in the anti-Stokes frequency channel at the detector can now be written as:

$$I(\omega_{as}) = \frac{\epsilon_0 c}{2} |E_{as}^{(3)} + E_{as}^{lo}|^2 \\ \propto |E_{as}^{(3)}|^2 + |E_{as}^{lo}|^2 + \left[\{E_{as}^{(3)}\}^* E_{as}^{lo} + \{E_{as}^{lo}\}^* E_{as}^{(3)} \right] \quad (1.29)$$

where E_{as}^{lo} is the local oscillator field at the anti-Stokes frequency. The last term on the right hand side of Equation 1.29 represents a heterodyne mixing contribution that depends on both the nonlinear anti-Stokes field $E_{as}^{(3)}$ and the local oscillator field. The heterodyne contribution I^{het} can be recast as:

$$\begin{aligned} I^{het}(\omega_{as}) &= 2A_{as}^{lo} \left[\text{Re}\{E_{as}^{(3)}\} \cos\phi + \text{Im}\{E_{as}^{(3)}\} \sin\phi \right] \\ &= 2\alpha [\text{Re}\{\chi_{NL}\} \cos(\phi - \phi_p) + \text{Im}\{\chi_{NL}\} \sin(\phi - \phi_p)] \end{aligned} \quad (1.30)$$

where

$$\alpha = |A_{as}^{lo} A_1^2 A_2|$$

A_{as}^{lo} is the amplitude of the local oscillator

The phase difference between $E_{as}^{(3)}$ field and the (real) E_{as}^{lo} field is indicated as ϕ , whereas the phase difference between the radiated field $E_{as}^{(3)}$ and the induced polarization $P(\omega_{as})$ is indicated as ϕ_p . Let us consider the energy flow of the heterodyne detected signal under the condition of driving the oscillator at the vibrational resonance frequency, i.e., $\Omega = \omega_v$. In this situation, we see from Equation 1.21 that χ_{NL} is purely imaginary in case nonresonant contributions to the nonlinear susceptibility are ignored. The total detected intensity in the anti-Stokes channel is then:

$$I(\omega_{as}) \propto |E_{as}^{(3)}|^2 + |E_{as}^{lo}|^2 + 2\alpha \text{Im}\{\chi_{NL}\} \sin(\phi - \phi_p) \quad (1.31)$$

This result indicates that the detected intensity depends on the phase difference $\Delta\phi = \phi - \phi_p$. The actual geometrical phase difference between the induced field and the local oscillator depends on propagation factors that are not included in this simple interference model. In Chapter 2, we will consider a more complete description of the phase difference between $E_{as}^{(3)}$ and E_{as}^{lo} at the location of the detector in the context of light propagation. Here, we will use the simple interference model to briefly discuss several values for $\Delta\phi$ that correspond to important cases in the heterodyne detection scheme. For instance, when $\Delta\phi = 0$, the heterodyne term disappears and the total intensity is simply the sum of the (homodyne) anti-Stokes contribution and the local oscillator intensity. However, when $\Delta\phi = -\pi/2$, the heterodyne term is negative and the total energy detected in the anti-Stokes channel is less than the sum of the homodyne contributions ($\text{Im}\{\chi_{NL}\} > 0$; see Equation 1.21). Under these conditions, the CARS process is no longer purely parametric as dissipative interactions, which here scale with $\text{Im}\{\chi_{NL}\}$, also play a role. In case modulation techniques are employed, the heterodyne term can be selectively detected and the resulting signal is directly proportional to $\text{Im}\{\chi_{NL}\}$, the dissipative part of the coherent Raman interaction. The same detection strategy can also be applied to CSRS.

The example in the preceding text illustrates that for a particular coherent Raman process the presence of a phase coherent local oscillator can change the sensitivity of the measurement in terms of probing parametric and dissipative processes. This notion is important when describing the SRL and SRG processes. In SRL, the signal is detected in the ω_1 frequency channel. In this channel, $P(\omega_1)$ is the source of the nonlinear field $E_1^{(3)}$.

Because the frequency of the nonlinear radiation is similar to the frequency of the fundamental light field E_1 , interference between the two fields will occur. The fundamental E_1 field can be interpreted as a local oscillator. The total intensity detected in the ω_1 channel is:

$$I(\omega_1) = \frac{\epsilon_0 c}{2} \left| E_1^{(3)} + E_1 \right|^2 \\ \propto \left| E_1^{(3)} \right|^2 + \left| E_1 \right|^2 + 2\beta [\text{Re}\{\chi_{NL}\} \cos \Delta\phi + \text{Im}\{\chi_{NL}\} \sin \Delta\phi] \quad (1.32)$$

with $\beta = I_1 I_2$. At the far field detector, the phase shift $\Delta\phi$ amounts to $-\pi/2$, which implies that the real part of the material response is $\pi/2$ retarded with respect to the E_1 , while the imaginary part of the material response is out-of-phase with E_1 (see Chapter 2). We thus find:

$$I(\omega_1) \propto \left| E_1^{(3)} \right|^2 + \left| E_1 \right|^2 - 2\beta \text{Im}\{\chi_{NL}\} \quad (1.33)$$

Equation 1.33 thus shows that the total intensity in the ω_1 channel is attenuated because of the presence of the driven oscillator. The loss in the ω_1 channel is the result of destructive interference between the induced field and the fundamental field. Note that the attenuation is mediated by the dissipative part of the interaction as described by the imaginary part of the nonlinear susceptibility. In the ω_2 channel, the E_2 excitation field acts as the local oscillator. Using $\Delta\phi = \pi/2$ and $\chi_{NL}^* = -\chi_{NL}$ at the vibrational resonance, we find:

$$I(\omega_2) \propto \left| E_2^{(3)} \right|^2 + \left| E_2 \right|^2 + 2\beta \text{Im}\{\chi_{NL}\} \quad (1.34)$$

From Equation 1.34 we see that the intensity in the ω_2 channel grows. The gain in the ω_2 channel is due to constructive interference between the induced field and the driving field E_2 . When modulation techniques are used, the heterodyne portion of the signal can be separately detected and the resulting SRG signal is directly proportional to the dissipative part of the coherent Raman interaction.

The general picture offered by the classical model is that the harmonic oscillator, driven at ω_v , forms a material modulation that affects the amplitude of the fundamental fields E_1 and E_2 . The material modulation gives rise to frequency-shifted radiation at $\omega_1 + \omega_v$ and $\omega_2 - \omega_v$, the CARS and CSRS contributions, respectively. In the homodyne detection mode, the CARS and CSRS signals are sensitive to the parametric part of the interaction. On the other hand, the field contributions at $\omega_1 - \omega_v$ and $\omega_2 + \omega_v$ radiate in the ω_2 and ω_1 frequency channels, respectively, and interference between the nonlinear fields and the fundamental fields will occur. In the SRG channel this interference is constructive, producing a gain of the overall ω_2 field, whereas in the SRL channel the interference is destructive, giving rise to a loss of the amplitude of the ω_1 field. The extend of the loss and gain scales with $\text{Im}\{\chi_{NL}\}$, which describes the dissipative part of the interaction.

1.6 Semi-Classical Description: Quantum Matter and Classical Fields

The fully classical model provides a qualitative description of the coherent Raman process in which the nuclear motion is described as a harmonic oscillator. A shortcoming of the classical model is that it does not recognize the quantized nature of the nuclear oscillations. The semi-classical model incorporates the quantum mechanical character of the material into the picture, whereas the description of the field remains classical and hence the name semi-classical. As such, nonlinear susceptibilities can be derived that describe the accessible states of the nuclear mode and the transitions between these states, expressed in material parameters such as transition dipole moments. By including the quantum mechanical material properties, the semi-classical model predicts nonlinear susceptibilities that are quantitatively more meaningful. It also naturally describes the existence of nonresonant contributions to the nonlinear optical response.

1.6.1 Wavefunctions of Matter

In the quantum mechanical description, the state of the material is described in terms of molecular wavefunctions. The wavefunctions are a function of space and time and are generally written as a superposition of molecular eigenstates ψ_n :

$$\psi(r, t) = \sum_n c_n \psi_n(r, t) \quad (1.35)$$

where the c_n are the projections of ψ along the system's eigenstates. The r coordinate includes both the electronic and nuclear coordinates. The evolution of the wavefunction over time is given by the time-dependent Schrödinger equation:

$$i\hbar \frac{d\psi}{dt} = \hat{H}_0 \psi \quad (1.36)$$

Here \hat{H}_0 is the Hamiltonian of the system in the absence of any external field. The hat indicates that \hat{H}_0 is an operator. Because ψ_n are eigenstates of the unperturbed Hamiltonian, their evolution can be expressed as:

$$\psi_n(r, t) = a_n(r) e^{-i\omega_n t} \quad (1.37)$$

where

$a_n(r)$ denotes the spatially varying part of the wavefunction
 ω_n is the eigenfrequency associated with eigenstate ψ_n

The system's wavefunction is affected by the coupling to an external field. The Hamiltonian is now given by:

$$\hat{H} = \hat{H}_0 + \hat{V}(t) \quad (1.38)$$

where the interaction Hamiltonian is given as:

$$\hat{V}(t) = -\hat{\mu} \cdot E(t) \quad (1.39)$$

The interaction with the electric field happens through the charged particles, electrons and nuclei, of the material, which are set in motion by the optical field applied at time t . In the dipole approximation, the extent of the interaction is described by the electric dipole operator:

$$\hat{\mu} = \sum_{\alpha} e_{\alpha} \hat{r}_{\alpha} \quad (1.40)$$

where the sum runs over both nuclei and electrons. Solving the wavefunction for this new Hamiltonian would allow the calculation of several observables. Since we are interested in calculating the optical response of the material, our target is to determine the polarization $P(t)$ of the material in a given volume V . Once the wavefunction is known, the polarization can be calculated from the expectation value of the dipole operator:

$$P(t) = N \langle \hat{\mu}(t) \rangle = N \langle \psi(r, t) | \hat{\mu} | \psi(r, t) \rangle \quad (1.41)$$

where

the bra $\langle \psi |$ and ket $|\psi\rangle$ notation is used

N is the number density in volume V

Finding the driven wavefunction is not trivial, however, and approximate methods have to be used. The most general approach is based on perturbation theory, where $\hat{V}(t)$ is treated as a perturbation and the wavefunction $\psi(r, t)$ is expanded to the n th order. Using the perturbation-corrected wavefunction in Equation 1.41 yields contributions to the polarization to various orders in the field. Collecting terms to third-order in the applied field with a coherent Raman resonance at $\omega_1 - \omega_2$ allows for the calculation of the quantum mechanical counterparts to the classical nonlinear susceptibilities given in Equation 1.21. Such a description, however, is rarely used because it is unable to properly account for broadening mechanisms of spectroscopic features due to coupling to other (bath) degrees of freedom. To include such broadening phenomena, a density matrix formalism is commonly employed, as we will briefly describe in the next section.

1.6.2 Density Matrix

The density matrix operator is defined as:

$$\hat{\rho}(t) \equiv |\psi(t)\rangle\langle\psi(t)| = \sum_{nm} \rho_{nm}(t) |n\rangle\langle m| \quad (1.42)$$

where $|n\rangle$ is the bra notation of the eigenstates of the unperturbed system. From the definition of the density matrix we see that it depends on the operator $|n\rangle\langle m|$, and the matrix elements $\rho_{nm} = \langle n | \hat{\rho} | m \rangle$. The diagonal elements of the density matrix, ρ_{nn} ,

give the probability that the system is in state $|n\rangle$, while the off-diagonal elements imply that the system is in a coherent superposition of eigenstates $|n\rangle$ and $|m\rangle$. We will call $|n\rangle\langle m|$ with $n \neq m$ the *coherence* and $\rho_{nm}(t)$ the time-dependent amplitude of this coherence. The description of the coherent Raman process in terms of coherences will prove useful for analyzing the different quantum pathway contributions to the overall signal.

The density operator evolves in the Schrödinger picture as:

$$\frac{d\hat{\rho}}{dt} = -\frac{i}{\hbar}[\hat{H}, \hat{\rho}] \quad (1.43)$$

where the Hamiltonian is defined as in Equation 1.38 and the brackets indicate the commutator operation of two operators \hat{A} and \hat{B} according to $[\hat{A}, \hat{B}] \equiv \hat{A}\hat{B} - \hat{B}\hat{A}$. As in the classical model, we are interested in calculating the polarization of the material in a given volume V . The expectation value of the electric dipole operator can be expressed in terms of the density operator as:

$$\langle \hat{\mu}(t) \rangle = \sum_{nm} \mu_{mn} \rho_{nm}(t) \equiv \text{tr}[\hat{\mu} \hat{\rho}(t)] \quad (1.44)$$

The tr symbol denotes the trace over the matrix elements of the operator product between the brackets. Similar to solving for the system's wavefunction, the density matrix of the system is found by a perturbation expansion of $\hat{\rho}(t)$ in powers of the electric field:

$$\hat{\rho}(t) = \rho^{(0)}(t) + \rho^{(1)}(t) + \rho^{(2)}(t) + \rho^{(3)}(t) + \dots \quad (1.45)$$

here $\rho^{(n)}$ is the n th order contribution in the electric field. The zeroth order contribution denotes the unperturbed density matrix at thermal equilibrium and is given as:

$$\rho^{(0)}(t) = \rho(-\infty) = \frac{e^{-\hat{H}/kT}}{\text{tr}\{e^{-\hat{H}/kT}\}} \quad (1.46)$$

where k is Boltzmann's constant. The perturbative expression of each of the components $\rho^{(n)}$ gets increasingly more complex with growing orders of n . It is, therefore, helpful to use alternative notation for writing these expressions in a more compact and insightful form. A common tool is the use of Liouville space operators, also known as superoperators. The action of the Liouville space operator \mathbb{H} and $\mathbb{V}(t)$ on an ordinary operator \hat{A} is defined through:

$$\mathbb{H}\hat{A} \equiv [\hat{H}, \hat{A}] \quad (1.47)$$

$$\mathbb{V}(t)\hat{A} \equiv [\hat{V}(t), \hat{A}] \quad (1.48)$$

With these definitions, the equation of motion of the density matrix operator can be rewritten as:

$$\frac{d\hat{\rho}}{dt} = -\frac{i}{\hbar} \mathbb{H}\hat{\rho} \quad (1.49)$$

To describe the coherent Raman interaction, we are interested in finding $\rho^{(3)}$, the density matrix contribution that is third order in the electric field. The derivation of $\rho^{(3)}$ is beyond the scope of this chapter, and the reader is referred to the existing literature for details [1,10,11]. Here we merely give the result of $\rho^{(3)}$ as predicted by perturbation theory. The Liouville space notation yields compact expressions for the third-order density matrix contribution:

$$\begin{aligned} \rho^{(3)}(t) = & \left(\frac{-i}{\hbar}\right)^3 \int_0^\infty d\tau_3 \int_0^\infty d\tau_2 \int_0^\infty d\tau_1 \\ & \times \mathbb{G}(\tau_3)\mathbb{V}(t-\tau_3)\mathbb{G}(\tau_2)\mathbb{V}(t-\tau_3-\tau_2)\mathbb{G}(\tau_1)\mathbb{V}(t-\tau_3-\tau_2-\tau_1)\rho(-\infty) \end{aligned} \quad (1.50)$$

where the time variables τ_n run over the interval between the application of a light field incident at t_{n-1} and a light field incident at t_n , as shown in **Figure 1.5**. The Liouville space Green's function $\mathbb{G}(\tau)$ describes the propagation of the material system in the absence of the light fields and is given as:

$$\mathbb{G}(\tau) \equiv \theta(\tau)e^{-i\mathbb{H}\tau/\hbar} \quad (1.51)$$

with $\theta(\tau)$ the Heavyside step function. Note that the expression for $\rho^{(3)}$ has an intuitive form: reading from right to left, the system starts out at thermal equilibrium $\rho(-\infty)$ and is subsequently perturbed by successive light fields as described by the \mathbb{V} operator. In between the light-matter interactions, the material system evolves according to the Green's function \mathbb{G} . Using the solution of $\rho^{(3)}(t)$ as given in Equation 1.50 we can proceed with the calculation of the expectation value of the third-order polarization. This will be discussed in the next section.

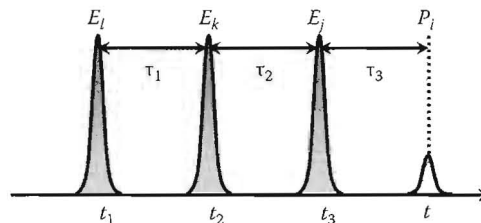


FIGURE 1.5 Schematic of the time ordering of the incident fields and the induced polarization.

1.6.3 Response Functions and Third-Order Susceptibility

1.6.3.1 Material Response Function

The polarization can be determined by evaluating the expectation value of the electric dipole operator as given in Equation 1.44. When the polarization is expanded in powers of the electric field, we find for the third-order contribution:

$$P^{(3)}(t) = N \text{tr}[\hat{\mu} \rho^{(3)}(t)] \quad (1.52)$$

Using Equation 1.50 we can express the components of the third-order polarization as:

$$P_i^{(3)}(t) = N \sum_{jkl} \int_0^\infty d\tau_3 \int_0^\infty d\tau_2 \int_0^\infty d\tau_1 R_{ijkl}^{(3)}(\tau_3, \tau_2, \tau_1) \\ \times E_j(t - \tau_3) E_k(t - \tau_3 - \tau_2) E_l(t - \tau_3 - \tau_2 - \tau_1) \quad (1.53)$$

where

the indices $\{i, j, k, l\}$ indicate the polarization orientation in cartesian coordinates $R_{ijkl}^{(3)}$ is the third-order response function, which is given as:

$$R_{ijkl}^{(3)}(\tau_3, \tau_2, \tau_1) = \left(\frac{i}{\hbar} \right)^3 \left\langle \hat{\mu}_i \mathbb{G}(\tau_3) \hat{\mu}_j^L \mathbb{G}(\tau_2) \hat{\mu}_k^L \mathbb{G}(\tau_1) \hat{\mu}_l^L \rho(-\infty) \right\rangle \quad (1.54)$$

where we have used the notation $\hat{\mu}^L$ to indicate the Liouville space version of the electric dipole operator $\hat{\mu}$. The response function describes the time-ordered response of the material to the incoming light fields. The expectation value in Equation 1.54 is to be taken over all the unperturbed eigenstates of the system. The expression of the nonlinear polarization in terms of a time-dependent response function is a natural means to describe time-resolved coherent Raman spectroscopy experiments. For many coherent Raman microscopy applications, however, the time-domain expression is of limited use, as the response is rarely time-resolved in fast imaging applications. Instead, the magnitude of the polarization at different vibrational frequencies is more practically related to imaging experiments. Therefore, we will seek frequency domain expressions of the nonlinear polarization.

To illustrate the form of the nonlinear polarization in the frequency domain, we will initially assume that the light fields are spectrally narrow, a situation directly relevant to picosecond coherent Raman microscopy. In this case we can write for the contribution to the nonlinear polarization that oscillates at the signal frequency $\omega_4 = \omega_1 + \omega_2 + \omega_3$:

$$P_i^{(3)}(t) = P_i(\omega_4) e^{-i\omega_4 t} + \text{c.c.} \quad (1.55)$$

Note that because $P_i^{(3)}(t)$ is a real function of time, the relation $P_i^*(\omega_4) = P_i^{(3)}(-\omega_4)$ must hold. The amplitude of the nonlinear polarization is given by:

$$P_i(\omega_4) = N \sum_{jkl} R_{ijkl}^{(3)}(\omega_4, \omega_1 + \omega_2, \omega_1) E_j(\omega_1) E_k(\omega_2) E_l(\omega_3) \quad (1.56)$$

with $R_{ijkl}^{(3)}$ the frequency domain response function defined through:

$$R_{ijkl}^{(3)}(\omega_4, \omega_1 + \omega_2, \omega_1) = \left(\frac{-1}{\hbar} \right)^3 \left\langle \hat{\mu}_i \mathbb{G}(\omega_4) \hat{\mu}_j^L \mathbb{G}(\omega_1 + \omega_2) \hat{\mu}_k^L \mathbb{G}(\omega_1) \hat{\mu}_l^L \rho(-\infty) \right\rangle \quad (1.57)$$

In this expression, we have used the frequency domain Green's function:

$$\mathbb{G}(\omega) = -i \int_0^{\infty} dt \mathbb{G}(t) e^{i\omega t} \quad (1.58)$$

The Green's function describes the frequency content of the density matrix during a given propagation period. The response function provides a detailed account of the evolution of the system in response to the incoming fields in terms of molecular coherences. In particular, the coherence during the second propagator is the material quantity that gives rise to the Raman sensitive signal. In the next section, we will focus on response functions that contain such propagators.

1.6.3.2 Third-Order Susceptibility

The system's response to a particular combination of optical frequencies is conveniently described by the third-order susceptibility $\chi_{ijkl}^{(3)}$. To obtain $\chi_{ijkl}^{(3)}$, we sum over all field permutations of $R_{ijkl}^{(3)}$. For instance, the $\chi_{ijkl}^{(3)}$ for the CARS process is defined through:

$$\chi_{ijkl}^{(3)}(-\omega_4; \omega_1, \omega_2, \omega_3) = -\frac{N}{6\epsilon_0} \sum_p R_{ijkl}^{(3)}(\omega_4, \omega_1 + \omega_2, \omega_1) \quad (1.59)$$

The summation indicated by p means that all frequency combinations, both positive and negative, of the applied fields are included that sum up to the final frequency ω_4 . The frequency arguments of $\chi_{ijkl}^{(3)}(-\omega_4; \omega_1, \omega_2, \omega_3)$ are organized as follows. Reading from left to right, the first frequency is the detected field. We will use a negative sign when the field is emitted and a positive sign when the field is absorbed. The fields to the right of the semicolon are the applied fields. In the frequency domain, the applied fields are not necessarily time-ordered.

The third-order susceptibility fully describes the response of material following the application of the fields E_1 , E_2 , and E_3 , and forms the link between experimental observations and the underlying material response. The third-order susceptibility contains many terms. Assuming that the material can be described by a four-level system as sketched in Figure 1.6 and all the molecules are initially in the ground state $|a\rangle$, the response function $R_{ijkl}^{(3)}$ consists of eight different quantum pathways [11]. Since there are $p = 3!$ different permutations of the incoming fields, the total number of terms in $\chi_{ijkl}^{(3)}(-\omega_4; \omega_1, \omega_2, \omega_3)$ is $3! \times 8 = 48$. Not all of these terms contribute to the vibrationally resonant coherent Raman response. To illustrate this point, we consider the CARS response where the signal is detected at the frequency $\omega_{as} = 2\omega_1 - \omega_2$. In this case, there are $p = 3$ different permutations of the incoming fields, producing a total of 24 terms to $\chi_{ijkl}^{(3)}(-\omega_{as}; \omega_1, -\omega_2, \omega_1)$. Together, these $\chi^{(3)}$ terms describe all the quantum pathways that

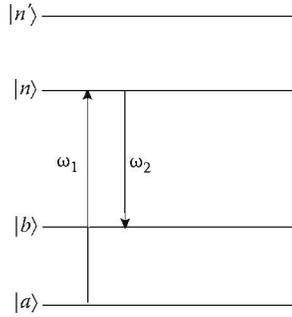


FIGURE 1.6 Energy diagram of the four-level system discussed in the text.

the system can make due to the perturbations induced by the applied fields ω_1 , $-\omega_2$ and ω_1 , and producing radiation at ω_{as} .

To gain physical insight into the form of $\chi^{(3)}$, we need to adopt a model for the evolution of the density matrix operator, which in turn determines the functional form of the Green's function propagator. The details of the propagation of the density matrix generally depend on the form of the system's Hamiltonian. Consequently, the evolution of the density matrix can be quite complex. Here we will not consider the complexities associated with elaborate models. Instead, we will focus only on a simple effective relaxation model that assumes that the elements of the time-dependent density matrix ρ_{nm} obey the following equation of motion in the absence of the fields:

$$\frac{d\rho_{nm}}{dt} = -i\omega_{nm}\rho_{nm} - \gamma_{nm}(\rho_{nm} - \rho_{nm}^{(0)}) \quad (1.60)$$

Here γ_{nm} is the dephasing rate associated with the nm transition, which depends on both relaxation and pure dephasing contributions. Using this simple model, the matrix elements of the frequency domain Green's function can be written as:

$$\mathbb{G}_{nm,nm}(\omega) = \frac{1}{\omega - \omega_{nm} + i\gamma_{nm}} \quad (1.61)$$

We can now write explicit expressions for the different $\chi_{ijkl}^{(3)}(-\omega_{as}; \omega_1, -\omega_2, \omega_1)$ terms that govern the CARS response. These terms are conveniently depicted by Feynman diagrams, some of which are given in Figure 1.7. The diagram in Figure 1.7a, for instance, represents the following term:

$$-\frac{N}{6\hbar^3 \epsilon_0} \sum_{ab,nn'} \rho_{aa}^{(0)} \frac{\mu_{an'}^i \mu_{n'b}^l \mu_{bn}^k \mu_{na}^j}{[\omega_{as} - \omega_{n'a} + i\gamma_{n'a}] [(\omega_1 - \omega_2) - \omega_{ba} + i\gamma_{ba}] [\omega_1 - \omega_{na} + i\gamma_{na}]} \quad (1.62)$$

It can be seen from Equation 1.62 that the contributions to $\chi^{(3)}$ become more significant when the denominator terms are minimized. The second denominator, representing

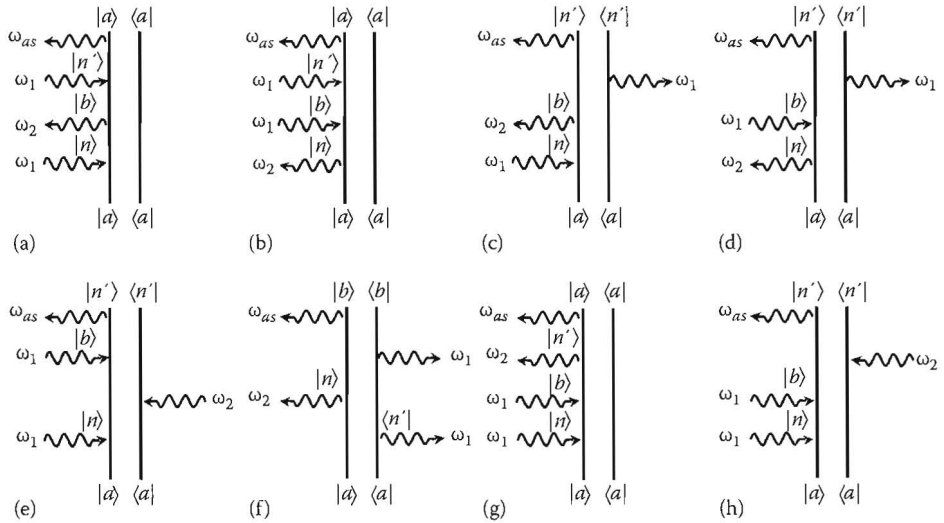


FIGURE 1.7 Double-sided Feynman diagrams of various contributions to $\chi^{(3)}(-\omega_{as}; \omega_1, -\omega_2, \omega_1)$. (a–d) Diagrams with a two-photon Raman resonance. (e through h) Diagrams without a two-photon Raman resonance. See Ref. [11] for details about Feynman diagrams.

the propagation of the density matrix after two field interactions, is minimized whenever the difference frequency $\omega_1 - \omega_2$ matches a vibrational frequency ω_{ba} . This is the Raman resonance condition. Figure 1.7b through d also contain a two-photon Raman resonance and thus contribute to the vibrationally resonant portion of $\chi^{(3)}(-\omega_{as})$. The contributions represented by Figure 1.7e through h, however, do not exhibit a Raman coherence at ω_{ba} after two field interactions, and the Raman resonance condition is not fulfilled. In the absence of electronic resonances, the contribution of a nonresonant diagram is generally less than that of a vibrationally resonant diagram. There are 16 more such nonresonant diagrams. The total contribution of the combined nonresonant terms is commonly indicated by $\chi_{NR}^{(3)}$, which is typically not negligible. We thus see that the semi-classical model provides a physical explanation for the existence of the nonresonant background: these are the quantum pathways the system can undergo which contribute to the dipole radiation at ω_{as} but do not contain propagators at $\omega_1 - \omega_2$ in resonance with the vibrational mode.

Besides the two-photon Raman resonances, $\chi^{(3)}(-\omega_{as})$ can contain additional resonances. Inspection of Equation 1.62 reveals that resonance conditions are achieved when the first and third terms in the denominator are minimized. Such conditions are met if ω_1 and/or ω_{as} are in resonance with an electronic state of the material. In addition, if the vibrational state $|b\rangle$ is initially populated, electronic resonances with ω_2 can also contribute to $\chi^{(3)}(-\omega_{as})$. These one-photon electronic resonances can boost the magnitude of $\chi^{(3)}(-\omega_{as})$ significantly. When both two-photon Raman resonances and electronic resonances are present, the vibrational information contained in the nonlinear susceptibility is enhanced by the electronic resonance. Resonance enhanced CARS (RCARS), which makes use of this enhancement mechanism, generally has a much higher sensitivity than regular CARS. Vibrationally resonant signals from chromophores down to μM concentrations have been measured with RCARS [12,13].

Note that electronic resonances do not only enhance the Raman resonant terms in $\chi^{(3)}(-\omega_{as})$, but also the vibrationally nonresonant terms. In addition, vibrationally nonresonant terms containing electronic two-photon resonances can contribute significantly to the overall magnitude of $\chi^{(3)}$. Diagrams (g) and (h) in Figure 1.7 contain such resonances whenever the molecule or medium contains transitions that match the combination frequency $\omega_1 + \omega_1$. The contribution of diagram (h), for instance, is:

$$\frac{N}{6\hbar^3\epsilon_0} \sum_{ab,nn'} \rho_{aa}^{(0)} \frac{\mu_{an'}^i \mu_{n'b}^i \mu_{bn}^k \mu_{na}^j}{[\omega_{as} - \omega_{bn'} + i\gamma_{bn'}][(\omega_1 + \omega_1) - \omega_{ba} + i\gamma_{ba}][\omega_1 - \omega_{na} + i\gamma_{na}]} \quad (1.63)$$

which exhibits a two-photon resonance when the system has a two-photon accessible state such that $2\omega_1 = \omega_{ba}$ (note that b is a dummy index that is summed over all states).

In CRS microscopy, we are typically concerned with vibrational resonances of non-absorbing molecules. In this case, it is not very practical to interpret the experiment in terms of the full structure of $\chi^{(3)}$. For this purpose, the third-order susceptibility is often written in a shorthand notation that highlights only the relevant vibrational resonances contained in the second propagator:

$$\chi^{(3)}(-\omega_{as}; \omega_1, -\omega_2, \omega_1) = \chi_{NR}^{(3)} - \sum_b \frac{A_b}{(\omega_1 - \omega_2) - \omega_{ba} + i\gamma_{ba}} \quad (1.64)$$

where all vibrationally nonresonant terms, including terms with two-photon electronic resonances, are lumped into $\chi_{NR}^{(3)}$. The second term on the right hand side of the equation is the vibrationally resonant contribution $\chi_R^{(3)}$ with A_b the effective amplitude associated with the ω_{ba} resonance.

1.6.3.3 Frequency Dependence of $\chi^{(3)}$

Many of the CRS imaging properties are directly related to the frequency dependence of $\chi^{(3)}$. The behavior of $\chi^{(3)}(-\omega_{as}; \omega_1, -\omega_2, \omega_1)$ as a function of the difference frequency $\Omega = \omega_1 - \omega_2$ near the ω_{ba} resonance is sketched in Figure 1.8. The imaginary part of the resonant portion of $\chi^{(3)}(\Omega)$ shows a maximum around the vibrational resonance frequency, whereas the real part features a dispersive profile. When expressed in terms of amplitude and phase, the nonlinear susceptibility displays the familiar behavior of a driven oscillator, where the phase of the oscillator with respect to the driving field undergoes a π step when the driving frequency is transitioning through resonance. This is illustrated in Figure 1.8b. The spectral phase behavior of $\chi^{(3)}$ plays an important role in CRS, and in CARS and CSRS in particular. The resonant nonlinear susceptibility produces a field that is interfering differently with the nonresonant field on each side of the resonance. On the low energy side, the resonant field is in phase with the (spectrally flat) nonresonant field contribution. On the high energy side of the resonance, the resonant field approaches a π phase shift relative to the nonresonant field, introducing destructive interference between the two contributions. The destructive interference is reflected in the $|\chi^{(3)}(\Omega)|^2$ spectrum as the dip on the high energy side of the spectral profile, as

1.7.1 Quantum Description of the Field

In the quantum-field description of the linear and nonlinear Raman interactions, the electric field is quantized. Similar to the material degrees, the optical electric field is described by a wavefunction, which we will denote as $|\Psi_F\rangle$. The expectation value of the field is given by the expectation value of the optical electric field operator, $\langle\Psi_F|\hat{E}(\mathbf{r},t)|\Psi_F\rangle$, where the operator is written as:

$$\hat{E}(\mathbf{r},t) = \hat{E}_s(\mathbf{r},t) + \hat{E}_s^\dagger(\mathbf{r},t) \quad (1.69)$$

with

$$\hat{E}_s(\mathbf{r},t) = \left(\frac{\hbar\omega_s}{2\epsilon_0 V}\right)^{1/2} \hat{a}_s e^{-i(\omega_s t - \mathbf{k}_s \cdot \mathbf{r})} \quad (1.70)$$

$$\hat{E}_s^\dagger(\mathbf{r},t) = \left(\frac{\hbar\omega_s}{2\epsilon_0 V}\right)^{1/2} \hat{a}_s^\dagger e^{i(\omega_s t - \mathbf{k}_s \cdot \mathbf{r})} \quad (1.71)$$

where

\hat{a}_s^\dagger and \hat{a}_s are the boson creation and annihilation operators for the mode s , respectively V is the quantization volume of the photon mode s [14,15]

The annihilation operator annihilates a photon from the mode s , while the creation operator creates a photon in the mode s :

$$\hat{a}_s^\dagger |\Psi_F^s(n)\rangle = n_s^{1/2} |\Psi_F^s(n+1)\rangle \quad (1.72)$$

$$\hat{a}_s |\Psi_F^s(n)\rangle = (n_s - 1)^{1/2} |\Psi_F^s(n-1)\rangle \quad (1.73)$$

where n_s , an integer, is the photon occupation number of mode s . The system's Hamiltonian now includes the contributions from the field in addition to the material degrees of freedom:

$$\hat{H} = \hat{H}_0 + \hat{H}_F + \hat{H}_{int} \quad (1.74)$$

where

\hat{H}_0 is the unperturbed Hamiltonian of the material as before

\hat{H}_F is the contribution from the field degrees

\hat{H}_{int} constitutes the interaction between the field and material

The latter two contributions are written in the quantum-field model as:

$$\hat{H}_F = \sum_s \hbar\omega_s \hat{a}_s^\dagger \hat{a}_s \quad (1.75)$$

$$\hat{H}_{int} = \hat{E}_s(\mathbf{r},t)\hat{V}^\dagger(\mathbf{r}) + \hat{E}_s^\dagger(\mathbf{r},t)\hat{V}(\mathbf{r}) \quad (1.76)$$

where the dipole operators are of the form:

$$\hat{V}(\mathbf{r}) = \sum_{\alpha=1}^N \delta(\mathbf{r} - \mathbf{r}_{\alpha}) \sum_{a,b>a} \mu_{ab} |a\rangle\langle b| \quad (1.77)$$

The index α runs over all molecules, which are assumed to be identical.

An important difference between the semi-classical approach and the quantum-field description is captured by the expression for \hat{H}_{int} in Equation 1.76: a field-matter interaction involves a change in both the material and the field degrees of freedom. In the classical and semi-classical approach, the signal is obtained by calculating the expectation value of the dipole operator to determine the material polarization, which then acts like a source for the detected radiation. The quantum-field method calculates the signal in a different fashion. Below we describe two quantum-field approaches for calculating the optical signals. These methods differ in their perspective: the first considers the signal from the field degrees point of view whereas the second method considers the signal from the perspective of the material degrees.

1.7.1.1 Field Perspective

In a first quantum-field approach, the signal is calculated by looking at the field. This method equates the optical signal directly to the change in the number of photons. The photon number in mode s is given by the expectation value of the photon occupation number operator, which is given by:

$$\hat{N}_s = \hat{a}_s^\dagger \hat{a}_s \quad (1.78)$$

The eigenvalues of \hat{N}_s correspond to the number of photons in mode s :

$$\hat{N}_s = \hat{a}_s^\dagger \hat{a}_s \left| \Psi_F^s(n) \right\rangle = n_s \left| \Psi_F^s(n) \right\rangle \quad (1.79)$$

The signal detected in this mode is then defined by:

$$S_s = \frac{d}{dt} \langle \hat{N}_s \rangle \quad (1.80)$$

We see that the signal in Equation 1.80 has a very intuitive form, as it simply represents the change in the number of photons of a certain frequency ω_s . The expectation value of the photon occupation number operator can be calculated by solving the density matrix for the total system $\hat{\rho}_{tot}(t)$, which now includes both material and field degrees. The signal then becomes:

$$\begin{aligned} S_s &= \frac{d}{dt} \text{tr}[\hat{N}_s \hat{\rho}_{tot}(t)] \\ &= -\frac{2}{\hbar} \text{Im}\{\text{tr}[\hat{E}_s(\mathbf{r}, t) \hat{V}^\dagger]\} \end{aligned} \quad (1.81)$$

In the next sections, we will use this expression to calculate the spontaneous Raman signal and the coherent Raman signals.

1.7.1.2 Material Perspective

In a second quantum-field approach, the material's perspective is chosen. Instead of focusing on changes in the photon number, the transitions between states in the material are explicitly considered. Because the field and material degrees are coupled, a transition between states implies a corresponding change in the field degrees, i.e., energy has been exchanged between the fields and the material. For this reason, this approach is only useful for the calculation of dissipative signals. The transition rate $R_{a \rightarrow n}$ between state $|a\rangle$ and state $|n\rangle$ is given by Fermi's golden rule as:

$$R_{a \rightarrow n} = \frac{2\pi}{\hbar^2} \sum_n \left| \langle n | \hat{H}_{int} | a \rangle \right|^2 \delta(\omega_n - \omega_a) \quad (1.82)$$

The term within brackets can be interpreted as the transition amplitude. This expression considers the transition between states as mediated by one-photon interactions only. Fermi's golden rule can be expanded in the field-matter interaction to include higher order photon processes. The rate of a k -photon process is given by a generalized Kramers–Heisenberg form [16]:

$$R_{a \rightarrow n} \propto \left| T_{na}^{(k)}(\omega_1, \dots, \omega_k) \right|^2 \delta\left(\sum_{i=1}^k \omega_i - \omega_{na}\right) \quad (1.83)$$

where $T_{na}^{(k)}$ are the k th-order transition amplitudes. The first three orders are given by:

$$T_{na}^{(1)}(\omega_{na}) = - \int d\omega_1 \tilde{T}_{na}^{(1)}(\omega_1) \delta(\omega_{na} - \omega_1) \quad (1.84)$$

$$\begin{aligned} T_{na}^{(2)}(\omega_{na}) &= \frac{2\epsilon_0}{\hbar} \int d\omega_1 d\omega_2 E(\omega_1) E(\omega_2) \\ &\quad \times \tilde{T}_{na}^{(2)}(\omega_1, \omega_2) \delta(\omega_{na} - \omega_1 - \omega_2) \end{aligned} \quad (1.85)$$

$$\begin{aligned} T_{na}^{(3)}(\omega_{na}) &= - \frac{4\epsilon_0^2}{\hbar^2} \int d\omega_1 d\omega_2 d\omega_3 E(\omega_1) E(\omega_2) E(\omega_3) \\ &\quad \times \tilde{T}_{na}^{(3)}(\omega_1, \omega_2, \omega_3) \delta(\omega_{na} - \omega_1 - \omega_2 - \omega_3) \end{aligned} \quad (1.86)$$

where $E(\omega_i)$ is the expectation value of the optical field operator and

$$\tilde{T}_{na}^{(1)}(\omega_1) = \mu_{na} \quad (1.87)$$

$$\tilde{T}_{na}^{(2)}(\omega_1, \omega_2) = \sum_v \frac{\mu_{nv} \mu_{va}}{\omega_1 - \omega_{va} + i\gamma} \quad (1.88)$$

$$\tilde{T}_{na}^{(3)}(\omega_1, \omega_2, \omega_3) = \sum_{v,w} \frac{\mu_{nw} \mu_{vw} \mu_{va}}{(\omega_1 + \omega_2 - \omega_{wa} + i\gamma)(\omega_1 - \omega_{va} + i\gamma)} \quad (1.89)$$

Because the field is quantized, the material transitions are directly correlated with the change in the number of photons. For a given photon mode s , we can thus write for the $a \rightarrow n$ transition:

$$S_s \propto \pm R_{a \rightarrow n} \quad (1.90)$$

where the minus sign indicates the emission of a ω_s photon and the plus sign the absorption of a ω_s photon.

The above description examines directly the transitions in a molecule, and thus provides an intuitive picture of the underlying physical process during the Raman excitation. Although the changes in the material degrees of freedom are coupled to changes in the field degrees of freedom, this description does not necessarily specify which particular field mode is affected. Hence, for processes that involve multiple field modes, additional information is required to determine which field modes are affected by the transitions in the material. Note also that the transition amplitude approach is not suitable to describe parametric processes such as homodyne-detected CARS, because of the lack of an effective molecular transition.

1.7.2 Quantum Description of Spontaneous Raman Scattering

The spontaneous Raman scattering process involves a strong driving field ω_1 and a spontaneously emitted field at ω_2 . The spontaneous emission process cannot be accounted for with a classical description of the field. Therefore, the expression obtained for the Raman signal in Equation 1.11 is inaccurate. The classical model is also unable to reveal the similarity between the field-matter interaction in the spontaneous Raman process and the interactions of a $\chi^{(3)}$ process. A quantum-field description of the scattering process provides new insights on both counts.

We will first calculate the Raman signal using Equation 1.81. Since the incoming optical field mode ω_1 is strong and relatively unattenuated by the Raman scattering process, this field can be treated as classical. The emitted field mode ω_2 is quantized, and its density matrix is initially in the vacuum state ($|\psi_F\rangle\langle\psi_F| = |0\rangle\langle 0|$). The lowest order density matrix operator that contributes to the signal S_2 is $\hat{\rho}_{tot}^{(3)}$, which involves two interactions with ω_1 and two interactions with ω_2 . The pathway of the density matrix that contributes to the incoherent Raman response is sketched in Figure 1.9. Similar to the Raman active $\chi^{(3)}$ processes, the system resides in an ab coherence after two field interactions. The final emission is at $\omega_2 = -\omega_1 + \omega_2 + \omega_1$. In this process, the density matrix of the ω_2 field has been raised from the vacuum state to the one photon state $|1\rangle\langle 1|$, which is the radiated photon. Based on this pathway, the incoherent spontaneous Raman emission rate is obtained from Equation 1.81 as:

$$S_2 = \frac{1}{\hbar^4} \sum_{k_2} \frac{\hbar\omega_2}{2\epsilon_0 V} 2 \text{Im} \{R(\omega_2, \omega_2 - \omega_1, -\omega_1)\} |E_1|^2 \quad (1.91)$$

where the sum is over all the ω_2 modes with wave vector k_2 within volume V . This equation shows that although the Raman response involves four field interactions, the

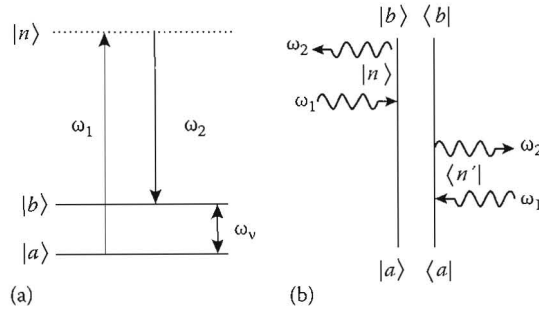


FIGURE 1.9 Quantum mechanical picture of the spontaneous Raman process. (a) Energy level diagram. (b) Double-sided Feynman diagram of the spontaneous light scattering response with a Raman resonance.

detected signal scales linearly with the intensity of the incident field $I_0 = |E_1|^2$. Using Equations 1.91 and 1.12, the strength of the Raman signal can also be expressed in terms of the differential Raman cross section:

$$\sigma(\omega_2) = \frac{1}{9} \frac{\omega_1 \omega_2^3}{\pi^2 \epsilon_0^2 \hbar^2 c^4} \text{Im} \{R(\omega_2, \omega_2 - \omega_1, -\omega_1)\} \quad (1.92)$$

The factor $1/9$ results from averaging over molecular orientations. We see that the Raman signal scales linearly with ω_1 and to the third power with ω_2 . The third-order power dependence includes the ω_2^2 dependence of the density of field modes in the cavity with volume V . The cross section can be approximated as:

$$\sigma(\omega_2) \simeq C_1 \text{Im} \{ \chi^{(3)}(\Omega) \} \quad (1.93)$$

where C_1 is a proportionality constant. This expression is an approximation because $\chi^{(3)}(\Omega)$ contains more pathways than the one that contributes to the spontaneous Raman process. Discrepancies may arise, for instance, in case of additional electronic resonances that may lift certain terms in the $\chi^{(3)}(\Omega)$ signal that are not part of the spontaneous Raman response. However, far from electronic resonances, only ground state Raman resonances contribute and Equation 1.93 generally holds.

The Raman response can alternatively be derived from the Kramers–Heisenberg formalism. At least two transitions are required to establish the $a \rightarrow b$ transition. The lowest order transition amplitude that describes this process is $T_{ba}^{(2)}$. The transition rate can then be written as:

$$R_{a \rightarrow b} \propto |T_{ba}^{(2)}(\omega_{ba})|^2 \delta(\omega_1 - \omega_2 - \omega_{ba}) \quad (1.94)$$

In this transition process, the ω_1 mode is changed from occupation number n to $n - 1$ (absorption), while the ω_2 mode changes from the vacuum state $|0\rangle$ to field state $|1\rangle$ (emission). The transition rate can then be recast as:

$$R_{a \rightarrow b} \propto \frac{\omega_1 \omega_2}{V^2} |E_1|^2 \left| \sum_n \frac{\mu_{bn} \mu_{na}}{\omega_1 - \omega_{na} + i\gamma} \right|^2 \delta(\omega_1 - \omega_2 - \omega_{ba}) \quad (1.95)$$

where E_1 is the expectation value of the field amplitude of the ω_1 mode. Accounting for the field mode density of the scattered field, we can deduce the differential cross section at the Raman resonance as:

$$\sigma(\omega_2) \propto \frac{\omega_1 \omega_2^3}{c^4} |\alpha|^2 \quad (1.96)$$

The transition amplitude α has the form of a (single pathway) Raman transition polarizability:

$$\alpha = \sum_n \frac{\mu_{bn} \mu_{na}}{\omega_1 - \omega_{na} + i\gamma} \quad (1.97)$$

In electronically resonant Raman experiments, the transition polarizability is large whenever the incident beam is close to an electronic transition of the molecule.

The virtue of this latter description is that it clearly shows what happens to the molecule. Before the interaction with the excitation field, the molecule is in its ground state $|a\rangle$. After the Raman scattering process, the molecule is in the vibrationally excited state $|b\rangle$. The molecule has thus gained energy in this process, during which one ω_1 photon was annihilated and one ω_2 photon was emitted. The energy gain of the molecule corresponds to the loss in the total light field, which amounts to $\hbar\omega_1 - \hbar\omega_2 = \hbar\omega_v$.

1.7.3 Quantum Description of Coherent Raman Signals: Interference of Pump-Probe Paths

From the previous section it is clear that the Raman process involves the transition from the ground state to the vibrational excited state in the molecule, while the total light field loses energy. This is a dissipative process, which under certain conditions is proportional to $\text{Im} \chi^{(3)}$, as shown in Equation 1.93. A similar analysis can be applied to interpret pump-probe type coherent Raman scattering signals (stimulated Raman scattering), which include the SRL and the SRG signals.

In SRL and SRG, we need to consider two field modes, ω_1 and ω_2 , both of which are initially occupied by photons. During the pump-probe process, an ω_1 mode is absorbed and an ω_2 mode is emitted, while the molecule undergoes a transition from the ground state a to the vibrationally excited state b . In SRL, the photon loss in the ω_1 mode is detected, whereas in SRG the photon gain in the ω_2 mode is detected. This process is identical to the Raman process sketched in Figure 1.9. The important difference between spontaneous Raman and stimulated Raman is that the ω_2 mode in the stimulated process is occupied, whereas it is empty in the spontaneous Raman case. The stimulated Raman process is dissipative and the signal can be written in a Kramers-Heisenberg form [16]. Selecting terms that contain the $\omega_{ba} = \omega_1 - \omega_2$ resonance and ignoring contributions from electronic resonances, the transition rate can be written as:

$$\begin{aligned} R_{a \rightarrow b} &\propto |E_1|^2 |E_2|^2 |\tilde{T}_{ba}^{(2)}|^2 \delta(\omega_1 - \omega_2 - \omega_{ba}) \\ &\propto \frac{\omega_1 \omega_2}{V^2} |E_1|^2 |E_2|^2 \left| \sum_n \frac{\mu_{bn} \mu_{na}}{\omega_1 - \omega_{na} + i\gamma} \right|^2 \delta(\omega_1 - \omega_2 - \omega_{ba}) \end{aligned} \quad (1.98)$$

Comparing the transition rate of the stimulated Raman process with the rate of the spontaneous Raman process in Equation 1.95, we see that the stimulated Raman process exhibits a higher rate due to the factor $|E_2|^2$. This is a direct consequence of the fact that the ω_2 mode is initially occupied, thereby enhancing the transition probability between the states a and b . The enhanced transition rate corresponds to an enhanced rate of change in the field modes, i.e., a higher rate of photon loss in the ω_1 detection channel and a higher rate of photon gain in the ω_2 channel. Consequently, as long as the stimulated Raman photon flux is above the shot-noise limit, the SRL and SRG optical signals from a particular molecular transition can be many orders of magnitude higher than the corresponding optical signals measured in a spontaneous Raman experiment.

1.7.4 Quantum Description of Heterodyne Coherent Raman Signals

Because homodyne-detected CARS probes a non-dissipative process, the corresponding signal cannot be written in a generalized Kramers–Heisenberg form. Heterodyne-detected CARS, on the other hand, can probe dissipative processes. In the following, we will discuss the case of the heterodyne CARS signal as it can be conveniently described within the quantum field framework of this chapter. The quantum field description allows for an intuitive interpretation of the dissipative and the parametric contributions to the CARS signal.

In the pump-probe type coherent Raman processes, we considered two field modes. In the heterodyne CARS experiment, the number of field modes is higher, introducing multiple pathways. Here, we consider the general case of four input modes, ω_1 , ω_2 , ω_3 , and ω_4 . We will assume that $\omega_1 - \omega_2 + \omega_3 = \omega_4$, and that $\omega_1 - \omega_2 = \omega_{ba}$ and $\omega_4 - \omega_3 = \omega_{ba}$. This situation is sketched in Figure 1.10. We will also assume that all modes have high photon occupation numbers.

We will first focus on the dissipative contribution from the material point of view. We will be concerned with pathways that contribute to an $a \rightarrow b$ transition in the molecule. In Figure 1.10a, we identify two pathways that mediate a transition

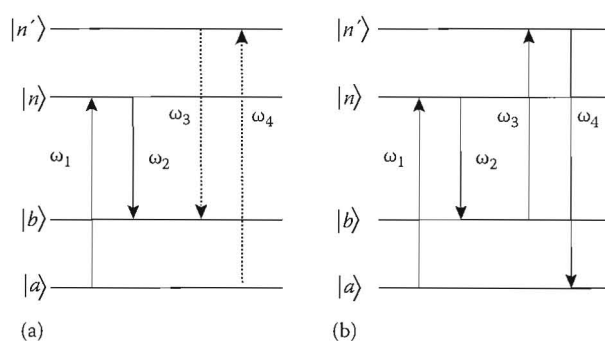


FIGURE 1.10 Energy level diagram representation of dissipative and parametric contributions in a heterodyne CARS experiment. (a) Dissipative contribution. Two $a \rightarrow b$ pathways can be distinguished: the $(\omega_1, -\omega_2)$ and the $(\omega_4, -\omega_3)$ pump-probe pathways, which constructively interfere. Both ω_1 and ω_4 photons are absorbed. (b) Parametric contribution. A photon in the ω_1 mode is absorbed and a photon in the ω_4 mode is emitted. The initial and final states of the molecule are the same, i.e., no effective $a \rightarrow b$ transition is made. Arrows are not time-ordered.

in the molecule. The first pathway, indicated by the solid arrows, is a pump-probe process in which one ω_1 photon is absorbed and one ω_2 photon emitted, leaving the molecule in the b vibrationally excited state. The second pathway, indicated by the dashed arrows, is a similar pump-probe process, in which one ω_4 photon is absorbed and one ω_3 photon emitted. The total transition *probability* in the heterodyne CARS experiment can be written as:

$$P_{a \rightarrow b} \propto |\mu_{bn}|^2 |\mu_{na}|^2 \left| \frac{E_1 E_2^*}{\omega_1 - \omega_{na} + i\gamma} \delta_{\Delta}(\omega_1 - \omega_2 - \omega_{ba}) + \frac{E_4 E_3^*}{\omega_4 - \omega_{na} + i\gamma} \delta_{\Delta}(\omega_4 - \omega_3 - \omega_{ba}) \right|^2 \quad (1.99)$$

where

E_i are the expectation values of the field operators

δ_{Δ} are slightly broadened delta functions

When calculating the square modulus, we find three processes that contribute to the dissipative signal:

$$P_{a \rightarrow b} = P_{a \rightarrow b}^{12} + P_{a \rightarrow b}^{34} + P_{a \rightarrow b}^{1234} \quad (1.100)$$

with

$$P_{a \rightarrow b}^{12} \propto |\mu_{bn}|^2 |\mu_{na}|^2 \left| \frac{E_1 E_2^*}{\omega_1 - \omega_{na} + i\gamma} \right|^2 \delta_{\Delta}^2(\omega_1 - \omega_2 - \omega_{ba}) \quad (1.101)$$

$$P_{a \rightarrow b}^{34} \propto |\mu_{bn}|^2 |\mu_{na}|^2 \left| \frac{E_4 E_3^*}{\omega_4 - \omega_{na} + i\gamma} \right|^2 \delta_{\Delta}^2(\omega_4 - \omega_3 - \omega_{ba}) \quad (1.102)$$

$$P_{a \rightarrow b}^{1234} \propto |\mu_{bn}|^2 |\mu_{na}|^2 2 \operatorname{Re} \left[\frac{E_1 E_2^* E_3 E_4^*}{(\omega_1 - \omega_{na} + i\gamma)(\omega_4 - \omega_{na} + i\gamma)} \right] \times \delta_{\Delta}(\omega_1 - \omega_2 - \omega_{ba}) \delta_{\Delta}(\omega_4 - \omega_3 - \omega_{ba}) \quad (1.103)$$

We see that first two processes are pump-probe type. $P_{a \rightarrow b}^{12}$ can be probed by detecting the loss in the ω_1 channel or the gain in the ω_2 channel. Similarly, $P_{a \rightarrow b}^{34}$ can be probed by detecting the loss in the ω_4 channel or the gain in the ω_3 channel. The third term is an interference term that represents the mutual interference of the two pump-probe pathways. The transition probability is higher when the two pathways are in phase and lower when the pathways are out of phase. Hence, by controlling the phase of the two pathways, the dissipative part of the signal can be either enhanced or suppressed.

In the CARS experiment, the ω_4 mode is detected, which we will denote as S_4 . We will next write the CARS signal in terms of transition amplitudes and identify the differences between the dissipative and parametric parts. The total signal can be written as:

$$S_4 = S_4^{dis} + S_4^{par} \quad (1.104)$$

The dissipative part of the heterodyne CARS signal is closely related to the interference term $P_{a \rightarrow b}^{1234}$ of the transition probability, and can be rewritten in terms of transition amplitudes. Assuming electronically off-resonance conditions and no thermal population in the vibrationally excited state, the dissipative signal can be written as [16]:

$$S_4^{dis} \propto \delta(\omega_1 - \omega_2 + \omega_3 - \omega_4) \delta(\omega_1 - \omega_2 - \omega_{ba}) \\ \times P(a) \left[E_1 E_2^* E_3 E_4^* \tilde{T}_{ba}^{(2)}(-\omega_2, \omega_1) \tilde{T}_{ba}^{(2)*}(-\omega_4, \omega_3) + \text{c.c.} \right] \quad (1.105)$$

where $P(a)$ is the equilibrium probability that the system is state a . From this expression it is evident that the dissipative CARS signal depends on the interference between two second-order transition processes. Note that, similar to spontaneous Raman and stimulated Raman scattering, the dissipative part is described by a product of two second-order transition amplitudes.

The parametric part to the signal, S_4^{par} , involves the process in which the initial and final states of the molecule are identical. This situation is sketched in **Figure 1.10b**. In this process, the second pathway is reversed. A ω_3 photon is absorbed and a ω_4 photon is emitted, bringing the molecule back into the initial state. The lowest order transition amplitudes that contribute to this process are $\tilde{T}_{aa}^{(4)}$, a four-photon scattering process. For the CARS channel, the relevant transition amplitude is proportional to $\tilde{T}_{aa}^{(4)}(-\omega_4, \omega_3, -\omega_2, \omega_1)$. The parametric signal is written as:

$$S_4^{par} \propto \delta(\omega_1 - \omega_2 + \omega_3 - \omega_4) P(a) \text{Im} \left\{ E_1 E_2^* E_3 E_4^* \right\} \text{Re} \left\{ \tilde{T}_{aa}^{(4)}(-\omega_4, \omega_3, -\omega_2, \omega_1) \right\} \quad (1.106)$$

We see that both the S_4^{dis} and S_4^{par} contributions to the heterodyne CARS signal have the expected linear dependence on the field amplitude E_4 , which corresponds to the classical local oscillator field. In addition, the quantum field description shows that the S_4^{dis} contribution necessarily consists of second-order scattering processes in which the $a \rightarrow b$ transition is made. The S_4^{par} contribution, on the other hand, is a fourth-order scattering process in which the molecule has not made an effective $a \rightarrow b$ transition. This latter information is not clearly expressed in the classical description, while the quantum field approach naturally shows the physical difference between the parametric and dissipative parts of the heterodyne CARS signal.

It is interesting to examine the parametric signal detected in other channels as well. In the ω_1 channel, which detects S_1^{par} , the relevant transition amplitude is $\tilde{T}_{aa}^{(4)}(\omega_4, -\omega_3, \omega_2, -\omega_1)$, which is of identical amplitude. However, in the parametric process, for each emitted ω_4 photon, there is an absorbed ω_1 photon. This implies that the detected parametric signals in these channels are related as $S_1^{par} = -S_4^{par}$. Note that the same relation does not hold for dissipative signals. The dissipative contribution in

CARS results from the photon pairs $(\omega_1, -\omega_2)$ and $(\omega_4, -\omega_3)$, in which both ω_1 and ω_4 are absorbed. These are two Stokes processes that constructively interfere. It is assumed that the heterodyne CARS experiment can be understood as the interference of two Stokes processes rather than an anti-Stokes process as the acronym implies. Hence, S_1^{dis} and S_4^{dis} have the same sign. From this simple relation we see that:

$$S_1 + S_4 = S_1^{dis} + S_4^{dis} \quad (1.107)$$

where the parametric signal is cancelled out. Measuring the photon change in the sum of both channels is thus equal to measuring only dissipative contributions to the coherent Raman process. The same relation holds for the S_2 and S_3 channels. More generally, the total dissipative signal D can be obtained by detecting all the modes simultaneously:

$$D = S_1 + S_2 + S_3 + S_4 \quad (1.108)$$

The interpretation of this latter result is straightforward: any energy loss in the combined field modes must correspond to an energy gain of the material, which constitutes the dissipative process.

1.8 Concluding Remarks

In this chapter, we have discussed the basics of the CRS process. We have seen that the classical, semi-classical, and quantum-field description each offer insight into several aspects of the CRS light-matter interaction. The classical model provides an intuitive picture in terms of oscillating electron clouds perturbed by harmonic nuclear modes. It offers a good framework for qualitatively interpreting the CRS signals measured in microscopy studies. The semi-classical model adds the actual quantum-mechanical mode structure of the molecule to the picture, which enables a direct connection between CRS experiments and quantum mechanical calculations of molecular vibrations. In addition, the semi-classical model offers a solid framework for dissecting ultrafast, time-resolved CRS experiments. Finally, the quantum-field approach takes into account the quantized energy exchange between light and matter. This latter description correctly predicts Raman cross sections and introduces additional insight into the origin of the parametric and dissipative contributions to the CRS signal.

Acknowledgments

E.O.P. acknowledges support from the National Science Foundation (NSF), grants CHE-0802913 and CHE-0847097. S.M. gratefully acknowledges support from the NSF, grant CHE-1058791, and the National Institutes of Health, grant GM059230 and 287 GM091364, and from the Department of Energy (DOE), Division of Chemical Sciences, Geosciences, and Biosciences, Office of Basic Energy Sciences.

References

1. R. W. Boyd, *Nonlinear Optics* (Academic Press, San Diego, CA, 2003).
2. D. Débarre and E. Beaurepaire, Quantitative characterization of biological liquids for third-harmonic generation microscopy, *Biophys. J.* **92**, 603–612 (2007).

3. G. R. Meredith, B. Buchalter, and C. Hanzlik, Third-order susceptibility determination by third harmonic generation. II, *J. Chem. Phys.* **78**, 1543–1551 (1983).
4. U. Gubler and C. Bosshard, Optical third-harmonic generation of fused silica in gas atmosphere: Absolute value of the third-order harmonic nonlinear optical susceptibility $\chi^{(3)}$, *Phys. Rev. B* **61**, 10702–10710 (2000).
5. T. Hashimoto, T. Yoko, and S. Sakka, Sol-gel preparation and third-order nonlinear optical properties of TiO₂ thin films, *Bull. Chem. Soc. Jpn.* **67**, 653–660 (1994).
6. Y. Wang, C. Y. Lin, A. Nikolaenko, V. Raghunathan, and E. O. Potma, Four-wave mixing microscopy of nanostructures, *Adv. Opt. Photon.* **3**, 1–52 (2011).
7. G. Placzek, Rayleigh-Streuung und Raman-Effekt, in *Handbuch der Radiologie*, E. Marx, Ed. (Akademische Verlagsgesellschaft, Leipzig, Germany, 1934).
8. E. Garmire, F. Pandarese, and C. T. Townes, Coherently driven molecular vibrations and light modulation, *Phys. Rev. Lett.* **11**, 160 (1963).
9. S. A. J. Druet and J. P. E. Taran, CARS spectroscopy, *Prog. Quantum Electron.* **7**, 1 (1981).
10. J. A. Armstrong, N. Bloembergen, J. Ducuing, and P. S. Pershan, Interactions between light waves in a nonlinear dielectric, *Phys. Rev.* **127**, 1918 (1962).
11. S. Mukamel, *Principles of Nonlinear Optical Spectroscopy* (Oxford University Press, New York, 1995).
12. L. A. Carreira, T. C. Maguire, and T. B. Malloy, Excitation profiles of the coherent anti-Stokes resonance Raman spectrum of β -carotene, *J. Chem. Phys.* **66**, 2621–2626 (1977).
13. W. Min, S. Lu, G. R. Holtom, and X. S. Xie, Triple-resonance coherent anti-Stokes Raman scattering microspectroscopy, *ChemPhysChem* **10**, 344–347 (2009).
14. R. Loudon, *The Quantum Theory of Light* (Oxford University Press, New York, 2000).
15. M. Scully and M. S. Zubairy, *Quantum Optics* (Cambridge University Press, Cambridge, U.K., 1997).
16. S. Mukamel and S. Rahav, Ultrafast nonlinear optical signals viewed from the molecule's perspective: Kramers–Heisenberg transition amplitudes versus susceptibilities, *Adv. Atom. Mol. Opt. Phys.* **59**, 233–263 (2010).